Structures, Energetics, and Spectra of (NH) and (OH) Tautomers of 2-(2-Hydroxyphenyl)-1-azaazulene: A Density Functional Theory/Time-Dependent Density Functional Theory Study

Asmaa B. El-Meligy, Safinaz H. El-Demerdash,* Mohamed A. Abdel-Rahman, Mohamed A. M. Mahmoud, Tetsuya Taketsugu, and Ahmed M. El-Nahas*

Read Online

ACCESS | Metrics & More | Article Recommendations | Supporting Information

ABSTRACT: Tautomerization of 2-(2-hydroxyphenyl)-1-azaazulene (**2OHPhAZ**) in the gas phase and ethanol has been studied using B3LYP, M06-2X, and ωB97XD density functional theory (DFT) with different basis sets. For more accurate data, energies were refined at CCSD(T)/6-311++G(2d,2p) in the gas phase. Nuclear magnetic resonance (NMR), aromaticity, Fukui functions, acidity, and basicity were also calculated and compared with experimental data. Time-dependent density functional theory (TDDFT)-solvation model based on density (TDDFT-SMD) calculations in acetonitrile have been utilized for the simulation of UV−vis electronic spectra. In addition, electronic structures of the investigated system have been discussed. The results reveal that the enol form (**2OHPhAZ**) is thermodynamically and kinetically stable relative to the keto tautomer (**2OPhAZ**) and different rotamers (**2OHPhAZ−R1:R3**) in the gas phase and ethanol. A comparison with the experiment illustrates a good agreement and supports the computational findings.
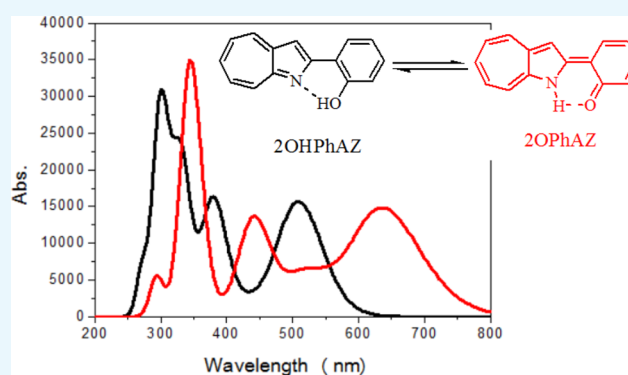
1. INTRODUCTION

Azulene, an isomeric structure of naphthalene (Scheme 1), has a fused five- and seven-membered ring.[1,2] It has a blue color

Scheme 1. Structures of Azulene, 1-Azaazulene, and Tautomeric Forms (Enolimine and Ketoenamine Form) of 2-(2-Hydroxyphenyl)-1-azaazulene
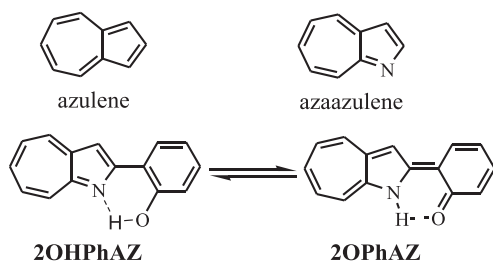
and high dipole moment.[3−6] This nonbenzenoid nonalternant structure attracts the interest of theoretical and experimental studies for its unusual photophysical properties.[7,8,17,9−16] Azulene derivatives have biological activities as well they can be anti-inflammatory[18] or have anti-cancer properties.[19]

Azaazulenes, an azulene heterocyclic analogue (Scheme 1), has attracted interest owing to their chemical and physical

properties and their biological activity[20,21] as anticancer agents.[22] 1-Azaazulenes is the most stable structure among the various structures of azaazulenes. Some 1-azaazulene derivatives have been used as ligands in metal complexes.[23−25] For example, 2-chloro-8-(2-pyridyl)-1-azaazulene acts as a bidentate ligand when reacted with Cu, Fe, and Pd ions and forms trigonal bipyramidal metal chelate complexes.[23]

1-Azaazulene with a phenol functional group at the 2-position has been synthesized by Oda et al.[26] This structure is similar to 8-hydroxyquinoline, which is an important chelating agent.[27,28] Thus, 2-(2-hydroxyphenyl)-1-azaazulene (**2OHPhAZ**) has the potential to be used as a chelating ligand through the imino nitrogen atom and the phenolic oxygen atom. **2OHPhAZ** has intense absorption in the visible region, and its long-wavelength absorption band shifts in the presence of several metal ions, and its emission upon excitation in the presence of Pb^{2+}, Al^{3+}, and Sc^{3+} ions is 10^3 times higher than

the quantum yield determined in the absence of ions, which suggests potential sensing of metal ions by this compound. A previous experimental study[26] reported the synthesis of **2OHPhAZ**, its X-ray crystallographic analysis, acidity, basicity, and UV–vis absorption, and emission spectra.

Tautomerism is a phenomenon of coexistence of two or more isomers of the same molecule. Many types of tautomerization can be found depending on the transferred atom. Our case study of tautomerism includes the transfer of hydrogen atom from one position to another within the same structure. In the system under consideration, such hydrogen transfer gives keto-enol tautomers. The intramolecular hydrogen transfer between two equilibrium structures exhibits extreme importance in pharmacology, organic chemistry, medicinal chemistry, and molecular biology.[29,30] Tautomers are formed by the exchange of hydrogen atoms between nitrogen and oxygen atoms of the heterocyclic ring. The proton transfer and hydrogen bonding are important characteristics of the hydrogen atom in chemistry. **2OHPhAZ** has hydroxyl substitution and azaazulenyl rings. Therefore, equilibrium between enolimine (phenol-imine, OH-form) and ketoenamine (C=O, NH-form) tautomeric forms is expected (Scheme 1).

Experimental studies on the subject of tautomerism are a challenging problem in chemistry and molecular biology. Most tautomers are not observed experimentally because of their low concentration. Detailed analysis of the structural and energetic parameters caused by the migration of hydrogen atoms would enable understanding different properties of tautomers. Knowledge of the relative stabilities of tautomeric forms and their mutual conversion represent an important issue from a structural chemistry point of view. Understanding physical and chemical properties of **2OHPhAZ** tautomers may assist future experimental studies on their potential use in some applications, particularly in metal complexes for analytical and biological applications. Comparing obtained results with experimental data[26] might give important information concerning the origin of the observed spectra and other properties. However, there is a lack of theoretical studies on **2OHPhAZ**.

In this work, we present a computational study on **2OHPhAZ** (Scheme 1) at the B3LYP/6-31G(d,p) level of theory. The relative stabilities and electronic absorption spectra of their tautomers and rotamers have been conducted using B3LYP, M06-2X, and ωB97XD functional using the 6-311++G(2d,2p) basis set at the B3LYP/6-31G(d,p) optimized structures in the gas phase and ethanol. Also, single point energy calculations at CCSD(T)[31,32]/6-311++G(2d,2p) in the gas phase have been performed. Two aspects here are important and will be addressed, namely, proton transfer and hydrogen bonding. A strong correlation exists between aromaticity and structure/stability and, therefore, aromaticity of tautomers and rotamers has also been examined in the light of nucleus-independent chemical shift (NICS) index[33,34] and harmonic oscillator model of aromaticity (HOMA).[35–37]

2. COMPUTATIONAL METHODS

Tautomers, rotamers, and transition states (TSs) for their interconversions were fully optimized at the density functional theory (DFT) of Becke's three-parameter and Lee–Yang–Parr hybrid functional (B3LYP)[38–40] in conjunction with the 6-31G(d,p) basis set. Vibrational frequency calculations have been conducted for each stationary point at the same level of optimization to characterize its nature as a minimum or transition state on the potential energy surface of the relevant systems. TSs were confirmed by the presence of one imaginary frequency that is examined using the ChemCraft 1.8 program.[41] Minima show real frequencies. The minimum energy path (MEP) was carried out at the level of optimization (B3LYP/6-31G(d,p)) through intrinsic reaction coordinate (IRC)[42,43] in order to verify that the located TSs connect the reactants and the desired products. It has been found that the energy of the transition state for tautomerization is higher than that of the keto form (**2OPhAZ**) because they include the zero-point correction. Energies were refined at B3LYP, meta hybrid generalized gradient approximation (M06-2X),[44,45] and long-range-corrected hybrid functional of Becke's 97 that include dispersion correction (ωB97XD)[46–49] functionals using the 6-311++G(2d,2p) basis set at the B3LYP/6-31G(d,p) optimized structures. For species in which a single-reference wavefunction is a good approximation, the CCSD-(T)[31,32] calculations represent a powerful tool for accurate reaction and activation energies. Therefore, we have conducted single point energy calculations at CCSD(T)/6-311++G-(2d,2p) using the B3LYP/6-31G(d,p) geometries. The zero-point-corrected relative energies (ΔE_0) reveal that M06-2X/6-311++G(2d,2p) has a slightly better performance than ωB97XD/6-311++G(2d,2p) relative to the more accurate (CCSD(T)/6-311++G(2d,2p)) level. Thus, unless noted otherwise, the M06-2X/6-311++G(2d,2p) level is used for the discussion of energetics.

Natural bond orbital (NBO) analysis[50,51] has been performed at B3LYP/6-31G(d,p) using NBO program version 3.1[52] to compute the atomic charges, orbital interactions, and their impact on the structure and stability of the investigated systems. Optimization of all investigated structures has also been conducted in ethanol at B3LYP/6-31G(d,p) using the solvation model based on density (SMD).[53] In addition, the single point solvation effect in ethanol has been calculated using M06-2X, B3LYP, and ωB97XD functionals with 6-311++G(2d,2p) basis sets at the B3LYP/6-31G(d,p)-optimized geometries in ethanol. All calculations were performed using the Gaussian 09 W program.[54]

Nuclear magnetic resonance (NMR) spectroscopy is a helpful tool for studying tautomeric equilibria. NMR shielding was calculated using the gauge-independent atomic orbital (GIAO) method,[55–57] relative to the ^{13}C and ^{1}H isotropic chemical shielding of tetramethylsilane (TMS), at B3LYP/6-31G(d,p) in chloroform using the optimized gas-phase geometry. These calculations yield the NICS[33,34] index that is used to evaluate aromaticity, antiartomaticity, and non-aromaticity of each ring for the structures under consideration and the corresponding TSs for their conversions. A ghost atom/probe (bq's) has been located at the center of the ring for determining NICS(0) and at 1 Å perpendicularly above the ring center for determining NICS(1).[33,34,58,59] Another criterion of aromaticity is the geometry-based index, HOMA,[35–37] which utilizes bond lengths according to the procedures given by Krygowski.[36]

To understand reactivity and stability of the studied structures, global chemical reactivity descriptors[60–63] have been determined using energies of highest occupied and lowest unoccupied molecular orbitals (HOMO and LUMO). Accordingly, ionization potential (IP), electron affinity (EA), absolute hardness (η), softness (S), electronegativity (χ), chemical potential (μ), and electrophilicity index (ω) were
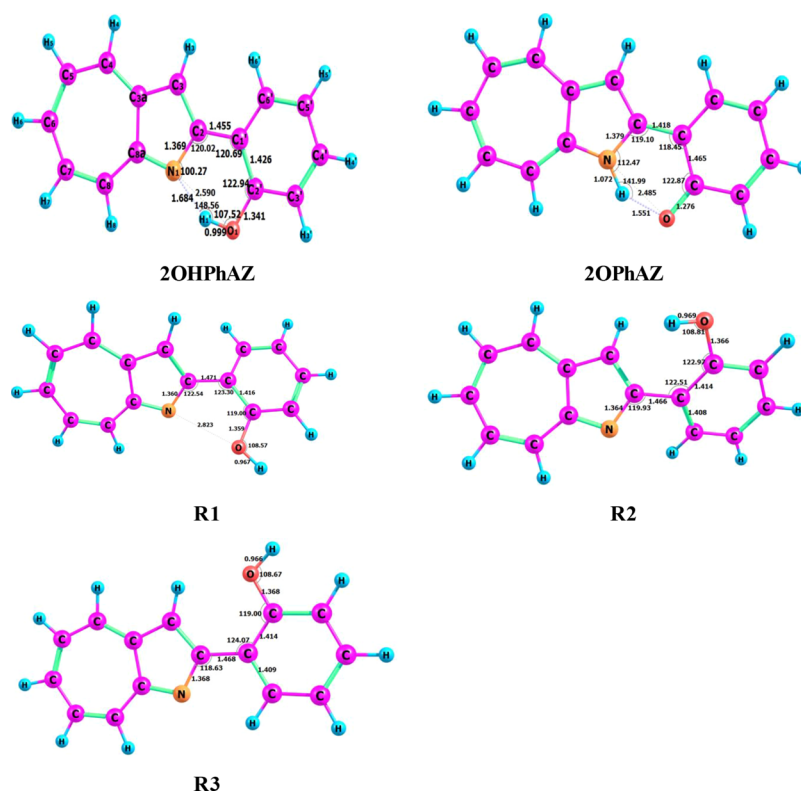
Figure 1. Optimized structures of the **2OHPhAZ** tautomers and rotamers at B3LYP/6-31G(d,p).

computed at B3LYP/6-31G(d,p) in the gas phase. The global chemical reactivity descriptors have been calculated using the following equations:

$$IP = -E_{HOMO} \quad (1)$$

$$EA = -E_{LUMO} \quad (2)$$

$$\eta = (E_{LUMO} - E_{HOMO})/2 \quad (3)$$

$$S = 1/2\eta \quad (4)$$

$$\chi = -(E_{LUMO} + E_{HOMO})/2 \quad (5)$$

$$\mu = (E_{LUMO} + E_{HOMO})/2 \quad (6)$$

$$\omega = \mu^2/2\eta \quad (7)$$

The Fukui function represents one of the density functional descriptors used to model chemical reactivity and site selectivity.[64] UCA-FUKUI software[65] has been used to calculate condensed Fukui functions (CFF) $f^+(r)$, $f^-(r)$, and $f^0(r)$ of the studied structures using atomic populations purposed by natural population analysis (NPA). Fukui functions are calculated utilizing the following equations:

$$f^+(r) = q_r(N + 1) - q_r(N) \text{ for nucleophilic attack} \quad (8)$$

$$f^-(r) = q_r(N) - q_r(N - 1) \text{ for electrophilic attack} \quad (9)$$

$$f^0(r) = q_r(N + 1) - q_r(N - 1) \text{ for radical attack} \quad (10)$$

where +, −, and 0 denote the nucleophilic, electrophilic, and radical attack, respectively.

Chattaraj et al. proposed the concept of generalized philicity[66] containing information about known various global and local reactivity. The dual descriptor $\Delta f(r)$ is the difference between nucleophilic and electrophilic attack in the Fukui function. If $\Delta f(r)$ is larger than zero at the specific site, this site will be favored for nucleophilic attack. To understand stability and reactivity of the studied structures, chemical reactivity toward positive and negative charges can be predicted through mapping the ESP.

Electronic absorption spectra for the studied structures were calculated at TD-DFT PBE[67,68] (TD-PBE/6-311+G(d,p)) in acetonitrile using the SMD approach at the B3LYP/6-31G(d,p)-optimized gas-phase geometry. The Perdew−Burke−Ernzerhof method (PBE0)[69] accurately estimated electron excitations of most organic dyes.[70] However, for the molecule under consideration compared to experimental results, it underestimates λ_{max} by 59 nm, whereas the PBE functional slightly overestimates λ_{max} by 11−13 nm depending on basis sets. The GaussSum program[71] was used to simulate the ultraviolet−visible (UV−vis) spectra. The natural transition orbitals (NTOs)[72] were analyzed for each electron excitation instead of particularly discussing the canonical orbitals. The frontier orbitals and NTOs were drawn using Chemcraft.[41]

3. RESULTS AND DISCUSSION

3.1. Structural Analysis. Five isomers are discussed for **2OHPhAZ**. The optimized structures of these forms are collected in Figure 1. Reliable structures are required in order to determine and rationalize the stability order of the investigated system. Gad et al.[16] reported that B3LYP/6-31+G(d,p) produces the same order of stability obtained by the ab initio multilevel CBS-QB3 method. Previous studies[44,45,73−77] illustrated high performance of M06-2X and ωB97XD functionals in predicting the trend of tautomers and conformer stability. Therefore, the structures will be discussed

Table 1. X-Ray and Calculated Geometrical Parameters of 2OHPhAZ at B3LYP/6-31G(d,p) in the Gas Phase and Ethanol

bond/angles[a,b]	exp.	gas phase	ethanol
N1−C2	1.365	1.369	1.370
C2−C3	1.401	1.415	1.409
C3−C3a	1.390	1.395	1.400
C3a−C4	1.388	1.404	1.404
C4−C5	1.378	1.388	1.389
C5−C6	1.394	1.405	1.404
C6−C7	1.382	1.393	1.395
C7−C8	1.386	1.399	1.398
C8−C8a	1.388	1.391	1.393
C8a−N1	1.353	1.349	1.353
C2−C1′	1.456	1.455	1.461
C1′−C2′	1.408	1.426	1.424
C2′−C3′	1.376	1.406	1.403
C3′−C4′	1.385	1.386	1.390
C4′−C5′	1.367	1.404	1.402
C5′−C6′	1.392	1.385	1.388
C6′−C1′	1.408	1.411	1.410
C2′−O	1.353	1.341	1.352
O−N1	2.583	2.590	2.572
O−H	0.975	0.999	1.007
N···H	1.688	1.684	1.653
O−H···N	150.740	148.563	149.579
N1−C2−C1′−C2′	0.829	−0.001	−0.009
C2−C1′−C2′−O1	−0.512	−0.003	−0.009
C1′−C2′−O1−H1	−2.175	−0.002	−0.008
RMSD		0.103	0.106

[a]Atom numbering is given in Figure 1. [b]Bond lengths (Å) and angles (in °).

at B3LYP/6-31G(d,p) and energies at M06-2X/6-311++G-(2d,2p), ωB97XD/6-311++G(2d,2p), and CCSD(T)/6-311++G(2d,2p). However, energies at B3LYP/6-31G(d,p) and B3LYP/6-311++G(2d,2p) are presented in the Supporting Information. To demonstrate the reliability of the obtained data, a comparison between the theory and the experiment has to be established. The geometrical parameters of **2OHPhAZ** optimized at B3LYP/6-31G(d,p) compared with the X-ray data of **2OHPhAZ**[26] are listed in Table 1. To measure geometrical similarities and differences between two structures, we used the root-mean-square deviation (RMSD).[78−81] The RMSD is calculated by the "RMS Compare Structures" utility in the ChemCraft program. A good agreement was recorded between the X-ray and the calculated **2OHPhAZ** structure in the gas phase and ethanol with RMSD values of 0.10 and 0.11 Å, respectively. Therefore, the B3LYP/6-31G (d,p) level well reproduces the X-ray structure. This supports the reliability of this level for structure optimization.

As displayed in Figure 1, the **2OHPhAZ** form shows an intramolecular hydrogen bond (IHB) between the hydrogen atom of the phenolic group and the nitrogen atom of the azaazulenyl moiety, (O−H···N, 1.68 Å); see Scheme 1. This value matches the H···N bond distance of 1.69 Å reported experimentally using ^{1}H NMR.[26] Also, the keto tautomer (**2OPhAZ**) illustrates an HB between the oxygen atom of the carbonyl group and the hydrogen attached to the nitrogen atom of the five-membered ring (N−H···O, 1.55 Å). The calculated donor−acceptor (O1−N1) distance of 2.59 Å in **2OHPhAZ** agrees very well with the experimental value (2.58
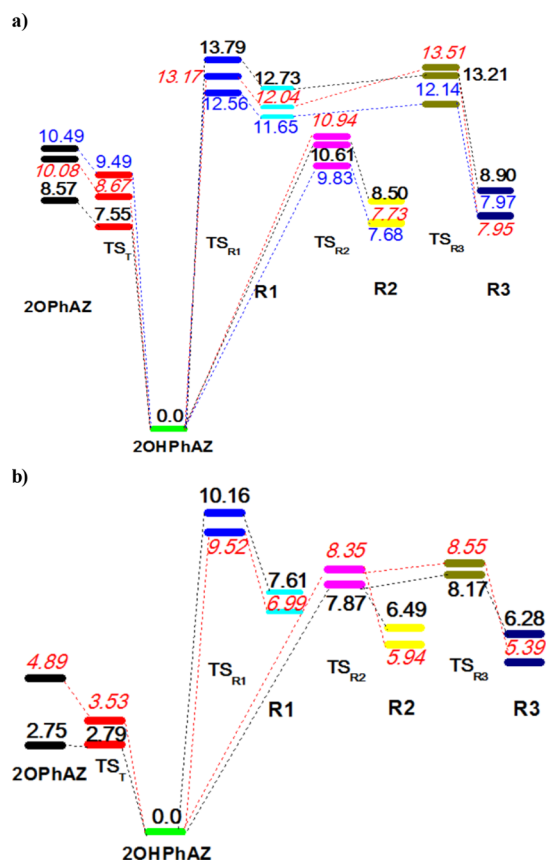

Figure 2. Potential energy diagram (ΔE_0, $\Delta E_0^{\ddagger}$, kcal/mol) for tautomerization and rotamerization of **2OHPhAZ** (a) in the gas phase and (b) in ethanol using the SMD solvation model at ωB97XD/6-311++G(2d,2p) (bold), M06-2X/6-311++G(2d,2p) (italic), and CCSD(T)/6-311++G(2d,2p) (normal) in the gas phase.

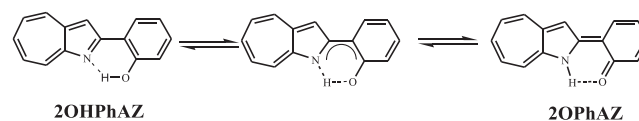**Scheme 2. RAHB in the 2OHPhAZ-2OPhAZ Tautomer**

Table 2. Relative Gibbs Free Energies (ΔG_{298}) and Gibbs Free Energy Barrier ($\Delta G_{298}^{\ddagger}$), in kcal/mol, and Dipole Moments (μ, in Debye) for the Tautomers and Rotamers of 2OHPhAZ in the Gas Phase and Ethanol at M06-2X/6-311++G(2d,2p) and CCSD(T)/6-311++G(2d,2p)

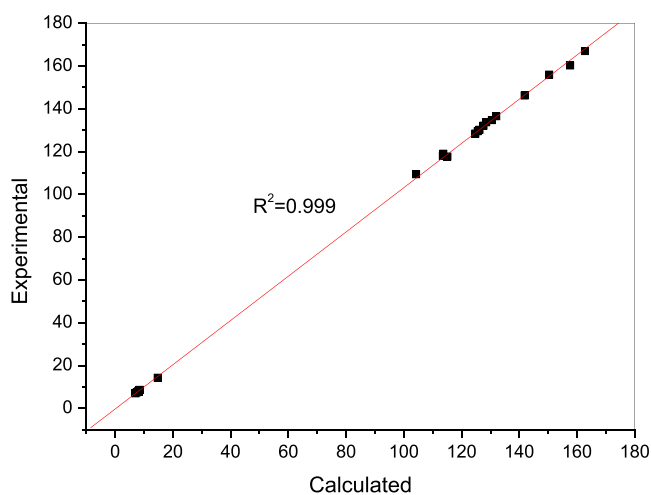|	gas phase				ethanol	
	M06-X[a]		CCSD(T)[a]		M06-2X[a]	
compound	ΔG_{298}	μ	ΔG_{298}	μ	ΔG_{298}	μ
2OHPhAZ	0.00	4.69	0.00	4.98	0.00	7.74
2OPhAZ	10.09	6.79	10.50	7.58	4.92	13.47
R1	11.49	1.20	11.10	1.36	6.72	2.75
R2	7.56	3.86	7.51	4.18	5.71	6.32
R3	7.48	2.11	7.50	2.10	4.82	3.77
TS_T	9.02	6.64	9.84	7.39	3.82	11.21
TS_R1	12.83	1.94	12.23	2.17	9.23	4.20
TS_R2	11.27	4.79	10.16	5.09	8.64	7.27
TS_R3	13.81	2.11	12.44	2.20	8.92	3.90

[a]Method/6-311++G(2d,2p)//B3LYP/6-31G(d,p).

Figure 3. Plot of the experimental chemical shifts verses the calculated ^{13}C and ^{1}H NMR chemical shifts at the B3LYP/6-31G(d,p) level of theory **2OHPhAZ** using the GIAO method in CHCl$_3$.

Table 3. ^{13}C and ^{1}H NMR Chemical Shifts (in ppm) for C2′ and H1 Attached to O/N at B3LYP/6-31G(d,p) for 2OHPhAZ Tautomers and Rotamers Using the GIAO Method in CHCl$_3$

	C2′	H1 attached to O/N
2OHPhAZ	157.64	14.76
2OPhAZ	171.33	19.40
R1	150.67	4.51
R2	150.87	5.97
R3	151.47	4.67

Å) and 2.49 Å in **2OPhAZ**. The HB strength in the tautomeric structures can be predicted from N−H···O, O−H···N, and O···N bond lengths.[82,83] As a result, the keto form has stronger HB, which might be attributed to the effect of the resonance-assisted hydrogen bond (RAHB).[35,84] The short donor−acceptor atom distance gives an indication about the existence of a low-barrier hydrogen bond (LBHB). The LBHB is biologically important[85] and is characterized by a short donor−acceptor distance of approximately between 2.4 and 2.6 Å.[83,86−88]

Three rotamers have been found for the enol isomer (**2OHPhAZ**), Figure 1. In the first rotamer, (**R1**), the OH bond adopts an anti-orientation with respect to the nitrogen atom. The other two rotamers (**R2** and **R3**) are obtained via rotation around the inter-cycle bond (C2−C1′) of **2OHPhAZ** and **R1**, respectively. In the **R1** rotamer, there is no hydrogen bond and, therefore, the donor−acceptor distance of 2.82 Å is longer than the corresponding distance of 2.59 Å in **2OHPhAZ**. In **R2** and **R3**, there are two stabilizing interactions that are absent in **R1**. These are attractive interaction between phenyl hydrogen with nitrogen and azulenyl hydrogen with oxygen. Both interactions exist in **R3** and the former one only in **R2**. Therefore, **R2** and **R3** are slightly more stable than **R1** at all levels.

Relative to the enol form, the calculated RMSD values for keto or rotamers in the gas phase are listed in Table S1. The RMSD value is larger for **R1** than the keto tautomer because of the different orientation of the hydroxyl group in the calculated **2OHPhAZ** structure, whereas **R2** and **R3** give the largest deviation.

Tautomerization and rotamerization pass through transitions states **TS$_T$**, **TS$_{R1}$**, **TS$_{R2}$**, and **TS$_{R3}$**. The optimized structures of

Table 4. NICS(1)$_{zz}$ (in ppm) and the HOMA Index of the Studied Tautomers and Rotamers Calculated at B3LYP/6-31G(d,p) in the Gas Phase and Ethanol[a]

compound		gas phase			ethanol		
		NICS(0)iso	NICS(1)$_{zz}$	HOMA	NICS(0)iso	NICS(1)$_{zz}$	HOMA
benzene		−9.84 (−8.06)[b]	−29.44 (−29.25)[b]	0.98 (0.99)[b]	−9.51	−28.59	0.98
pyrrole		−15.97 (−17.3)[c]	−29.80	0.92 (0.93)[d]	−15.75	−30.01	0.92
C$_7$H$_7$+		−6.81 (−6.7)[e]	−26.34	0.97	−6.87	−26.36	0.98
azulene	five-membered ring	−19.42 (−21.5)[c](−18.1)[f]	−44.70	0.29 (0.42)[g]	−19.23	−51.49	0.29
	seven-membered ring	−6.95 (−8.3)[c](−5.5)[f]	−21.07	0.52 (0.60)[g]	−6.84	−21.18	0.52
aza-azulene	five-membered ring	−16.89 (−15.0)[f]	−45.47	0.43	−16.66	−44.63	0.49
	seven-membered ring	−8.03 (−6.9)[f]	−24.43	0.60	−7.97	−24.61	0.65
2OHPhAZ	five-membered ring	−14.22	−34.83	0.47	−14.34	−34.83	0.53
	seven-membered ring	−6.79	−20.23	0.64	−7.15	−20.69	0.68
	six-membered ring	−8.11	−18.66	0.89	−8.33	−19.30	0.91
2OPhAZ	five-membered ring	−11.85	−26.67	0.53	−12.90	−29.20	0.61
	seven-membered ring	−3.49	−11.97	0.66	−5.00	−16.30	0.73
	six-membered ring	−3.69	−12.01	0.51	−4.73	−14.12	0.62
R1	five-membered ring	−14.44	−37.76	0.42	−14.44	−37.76	0.48
	seven-membered ring	−7.20	−22.16	0.61	−7.14	−22.33	0.65
	six-membered ring	−8.92	−18.36	0.94	−8.84	−18.45	0.93
R2	five-membered ring	−14.42	−36.26	0.45	−14.40	−35.96	0.51
	seven-membered ring	−7.16	−20.37	0.64	−7.15	−20.69	0.68
	six-membered ring	−8.77	−20.94	0.94	−8.80	−21.17	0.94
R3	five-membered ring	−14.90	−39.58	0.40	−14.66	−38.76	0.49
	seven-membered ring	−7.05	−21.52	0.62	−7.02	−21.67	0.66
	six-membered ring	−8.98	−22.25	0.94	−8.80	−22.20	0.93

[a]Five- and seven-membered rings of azaazulene and six-membered phenyl ring are given as presented in Figure 1. [b]Ref 109. [c]Ref 34. [d]Ref 110. [e]Ref 111. [f]Ref 114. [g]Ref 113.

Table 5. Global Chemical Descriptor (eV) of the Studied Structures at B3LYP/6-31G(d,p) in the Gas Phase

	E_{HOMO}	E_{LUMO}	E_g	IP	EA	χ	H	S	M	ω
2OHPhAZ	−5.46	−2.38	3.08	5.46	2.38	3.92	1.54	0.33	−3.92	4.99
2OPhAZ	−4.85	−2.55	2.30	4.85	2.55	3.70	1.15	0.43	−3.70	5.94
R1	−5.51	−2.04	3.47	5.51	2.04	3.77	1.74	0.29	−3.77	4.10
R2	−5.69	−2.34	3.35	5.69	2.34	4.01	1.68	0.30	−4.01	4.81
R3	−5.48	−2.06	3.43	5.48	2.06	3.77	1.71	0.29	−3.77	4.14

Table 6. NPA Charges of Some Selected Atoms[a] of the Investigated Systems Calculated at the B3LYP/6-31G(d,p) Level of Theory in the Gas Phase

	N	O	C2	C1′	C2′	H1
2OHPhAZ	−0.557	−0.701	0.229	−0.169	0.386	0.522
2OPhAZ	−0.543	−0.688	0.250	−0.202	0.439	0.486
R1	−0.466	−0.667	0.213	−0.125	0.368	0.489
R2	−0.560	−0.567	0.193	0.070	0.273	0.312
R3	−0.586	−0.562	0.234	0.055	0.284	0.318

[a]Atom numbering is given in Figure 1.

TS_T, TS_{R1}, TS_{R2}, and TS_{R3} for **2OHPhAZ** at B3LYP/6-31G(d,p) in the gas phase are presented in Figure S1. For **R2** and **R3** and their corresponding TSs, the dihedral angles of N1−C2−C1′−C2′, C2−C1′−C2′−O1, and C1′−C2′−O1−H1 are listed in Table S2. The breaking O−H bond in TS_T is stretched by 43.14% and the formed N−H bond is elongated by 33.79% with 0.146 Å of RMSD compared to **2OHPhAZ**. With respect to the **2OPhAZ** form, the breaking/forming, N−H/O−H bonds for TS_T are elongated/shortened by 4.01/7.80% with an RMSD equal to 0.027 Å. Therefore, the TS_T structure is closer to the structure of the keto form than the enol form. According to the Hammond postulate,[89] the transformation of the enol to keto form is endothermic. The donor−acceptor distance in the TS_T is lower than the corresponding values in enol and keto forms (2.44 Å). The O−H bond length in TS_{R1} and **R1** is comparable but shorter than that in **2OHPhAZ** by 0.03 Å because of the presence of HB in the latter structure. The H−O−C angle is rotated by 2.09° from **R1**. The donor−acceptor distance in the TS_{R1} is stretched to 2.88 Å.

3.2. Energies and Stability. The potential energy diagram for tautomerization and rotamerization of **2OHPhAZ** at ωB97XD/6−311++G(2d,2p), M06-2X/6-311++G(2d,2p), and CCSD(T)/6-311++G(2d,2p) levels of theory is illustrated in Figure 2a,b in the gas phase and ethanol, respectively. Energy profiles for tautomerization and rotamerization from IRC calculations at the B3LYP/6-31G(d,p) level are displayed in the Supporting Information (Figures S2 and S3, respectively). Compared to (CCSD(T)/6-311++G(2d,2p)) results, ωB97XD/6-311++G(2d,2p) and M06-2X/6-311++G-(2d,2p) exhibit a good agreement in reproducing ΔE_0 for **2OHPhAZ** tautomers and rotamers, with a slightly better performance of the latter method (see Figure 2). Therefore, we will continue our discussion at the M06-2X/6-311++G(2d,2p) level unless noted otherwise.

As displayed in Figures 2 and S2, ketonization and rotamerization of **2OHPhAZ** are endothermic processes that give further support for the experimental[26] finding of the **2OHPhAZ** enol form in the gas phase and ethanol solution as a thermodynamically most stable form (Figure 2a,b). It is more stable than the keto form by 10.08 (4.89) kcal/mol using the M06-2X/6-311++G(2d,2p) in the gas phase (ethanol). The

stability of the **2OHPhAZ** is expected from the aromaticity of the phenyl ring recorded in **2OHPhAZ** relative to the broken aromaticity in **2OPhAZ** (as will be discussed in Section 3.4). **2OHPhAZ** is also more stable than its rotamers **R1**, **R2**, and **R3** by 12.04 (6.99), 7.73 (5.94), and 7.95 (5.39) kcal/mol in the gas phase (ethanol), respectively. The stabilization of **2OHPhAZ** and **2OPhAZ** relative to the rotamers **R** can be rationalized in terms of the RAHB effect according to similar previous studies.[84,90−92]

In accordance with Scheme 2 as explained by Lenain et al.[84] for similar systems, the difference of stability **2OHPhAZ/2OPhAZ** is attributed to the direction of the π-electron delocalization that favors/hinders the proton transfer from the donor atom to the acceptor atom. This affects the relative stabilization or destabilization of the IHB. Thus, **2OPhAZ** is expected to have IHB that causes destabilization of the π-system.

From the calculated barrier heights for tautomerization, it can be noticed that IHB plays a vital role in the kinetic stability of the TS_T form in accordance with the results obtained by Garcia-Viloca et al. for the maleate anion.[93] The barrier from **2OPhAZ** to **2OHPhAZ** over TS_T equals −1.41 kcal/mol in the gas phase at M06-2X/6-311++G(2d,2p). Garcia-Viloca et al.[93] reported an energy barrier of −0.85 kcal/mol for the intramolecular proton transfer in the maleic monoanion calculated at MP2/6-31+G(d,p) in the gas phase. TS_T is considered as a mixture of two RAHB structures with the largest π-electron delocalization within the NCCCO quasi-ring and a higher covalent character of HBs that gives the explanation about the higher stability of TS over **2OPhAZ**. In the TS_T (Figure S3), the N1−H1 bond is formed gradually with the breaking of the O−H bond; the two curves cross each other near the transition state ($s = -0.4$ amu$^{1/2}$ bohr). The double bond of C−O and the single bond of N1−C2 are gently formed during the course of the reaction.

Determination of the equilibrium constant depends on Gibbs free energies (ΔG) for the investigated tautomers/rotamers according to $K = e^{(-\Delta G/RT)}$ relation, where K is the equilibrium constant, R is the universal gas constant, and T is the temperature in Kelvin. Relative Gibbs free energies (ΔG_{298}, $\Delta G_{298}^{\#}$) calculated at the M06-2X/6-311++G(2d,2p) and CCSD(T)/6-311++G(2d,2p) levels of theory are collected in Table 2, and those at the B3LYP/6-31G(d,p), B3LYP/6-311++G(2d,2p), and ωB97XD/6-311++G(2d,2p) levels are listed in Table S3. The values of ΔG_{298} give nearly the same order of stability for the investigated tautomers/rotamers as relative zero-point-corrected energies. It can be noticed that the energy differences in ethanol are higher than the corresponding results in the gas phase. This observation can be ascribed to the higher difference of dipole moments in ethanol than in the gas phase. The dipole moments of the studied tautomers/rotamers in the gas phase and in ethanol calculated at the M06-2X/6-311++G(2d,2p) levels of theory are also given in Table 2.

Table 7. Condensed Fukui Functions (f_k^+, f_k^-, f_k^0) of the Reactive Sites[a] Evaluated from Natural Population Analysis for the Investigated Tautomer and Rotamers at B3LYP/6-31G(d,p)

atom	2OHPhAZ			2OPhAZ			R1			R2			R3		
	f_k^-	f_k^+	f_k^0	f_k^-	f_k^+	f_k^0	f_k^-	f_k^+	f_k^0	f_k^-	f_k^+	f_k^0	f_k^-	f_k^+	f_k^0
N1	**0.0374**	-0.0937	0.0282	0.0239	-0.0802	0.0282	-0.0528	-0.0036	0.0282	-0.0345	0.0299	0.0023	-0.0237	0.0188	0.0024
H1	0.0031	**0.5219**	**0.2625**	0.0388	**0.4862**	**0.2625**	0.0362	**0.4887**	**0.2625**	0.0010	0.0000	0.0005	0.0205	-0.0073	0.0066
O1	-0.0194	-0.0576	0.0385	-0.0319	-0.0452	0.0385	-0.9348	-0.0237	0.0385	**0.9560**	**0.9560**	0.0106	-0.0333	**0.9640**	**0.4653**
C2	0.0222	0.0067	0.0144	0.0013	0.0276	0.0144	0.0396	-0.0099	0.0144	0.0396	-0.0139	0.0129	**0.0451**	-0.0155	0.0148
C3	0.0258	0.0159	0.0208	0.0188	0.0229	0.0208	**0.0440**	0.0077	0.0208	**0.0440**	-0.0628	0.0094	0.0292	-0.0008	0.0142
C4	0.0327	0.0563	**0.0445**	**0.0461**	**0.0428**	**0.0445**	0.0298	0.0591	**0.0445**	0.0309	0.0492	0.0400	0.0314	0.0503	0.0409
C5	0.0348	0.0163	0.0255	0.0207	0.0304	0.0255	**0.0442**	0.0068	0.0255	**0.0441**	0.0166	0.0303	**0.0458**	0.0093	0.0275
C6	**0.0406**	**0.0694**	**0.0550**	**0.0595**	**0.0506**	**0.0550**	0.0369	**0.0731**	**0.0550**	0.0373	0.0703	**0.0538**	0.0375	0.0678	0.0527
C7	0.0333	0.0123	0.0228	0.0118	0.0339	0.0228	**0.0454**	0.0003	0.0228	**0.0466**	0.0096	0.0281	**0.0479**	0.0035	0.0257
C8	0.0077	**0.0564**	0.0320	**0.0499**	0.0142	0.0320	-0.0046	0.0686	0.0320	-0.0069	0.0719	**0.0325**	-0.0058	0.0684	0.0313
C1'	0.0093	0.0285	0.0189	0.0425	-0.0047	0.0189	-0.0344	**0.0722**	0.0189	0.0818	-0.0707	0.0056	0.0199	-0.0697	0.0249
C2'	-0.0174	-0.0567	0.0370	-0.0706	-0.0035	0.0370	0.0011	-0.0751	0.0370	0.1316	-0.1869	0.0277	0.0242	-0.2072	0.0915
C3'	-0.0099	0.0292	0.0096	0.0002	0.0190	0.0096	0.0161	0.0031	0.0096	-0.5130	**0.5707**	0.0288	0.0217	**0.5713**	**0.2965**
C4'	**0.0361**	0.0367	0.0364	0.0350	0.0378	0.0364	**0.0431**	0.0297	0.0364	0.0377	0.0256	0.0316	0.0391	0.0257	0.0324
C5'	0.0300	0.0516	0.0408	0.0399	0.0417	0.0408	0.0226	0.0590	0.0408	**0.0456**	0.0378	**0.0417**	0.0173	0.0076	0.0124
C6'	0.0220	0.0156	0.0188	0.0264	0.0112	0.0188	0.0286	0.0090	0.0188	-0.5548	**0.5513**	0.0018	0.0271	**0.5524**	**0.2897**

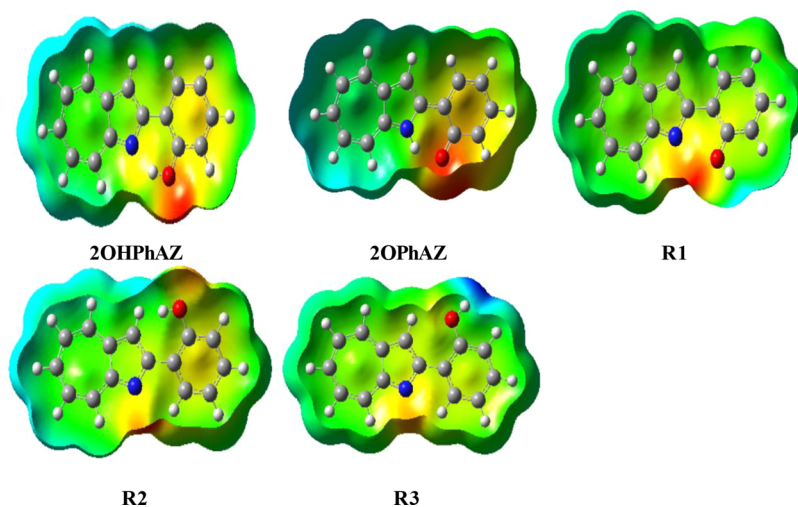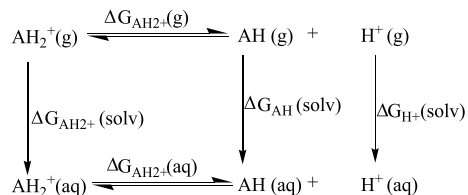[a] Atom numbering is given in Figure 1.

Figure 4. Molecular ESP surfaces of the investigated structure at B3LYP/6-31G(d,p).

Scheme 3. Thermodynamic Cycle Connecting Gas (g) and Aqueous (s) Phases for pK_a Calculation

3.3. NMR Analysis. LBHB can be investigated by NMR calculation.[94−96] In the NMR spectrum, the appearance of a low-field proton signal (high chemical shifts) is a well-known

effect of forming a hydrogen bond with a sign for an LBHB. The calculated ^{13}C and ^{1}H NMR chemical shifts for **2OHPhAZ** in CHCl$_3$ show good agreement with the experimental findings in CDCl$_3$. Plotting of the calculated ^{13}C and ^{1}H NMR chemical shifts against the experimental values of **2OHPhAZ** is displayed in Figure 3. A high correlation was noticed, which gives confidence on the used computational procedures. Detailed data about NMR of the studied tautomers and rotamers at B3LYP/6-31G(d,p) are summarized in Table S4. An inspection of Table 3 indicates that C$_2'$ in the **2OPhAZ** has the highest chemical shift (171.33 ppm) because of the electron-withdrawing effect of the attached oxygen atom of the carbonyl group. Apparently, H$_1$
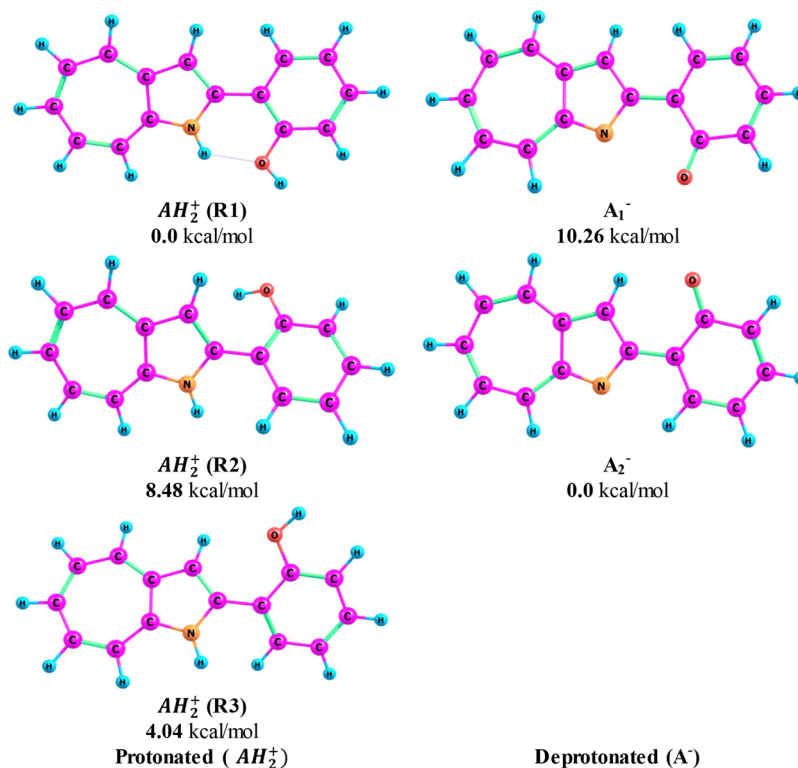

Figure 5. Optimized structures and the relative energy of protonated (AH$_2^+$, cation) and deprotonated (A$^-$, anion) forms of **2OHPhAZ** at B3LYP/6-31G(d,p).

**Table 8. Calculated Acidity Constant (pK_a) for the Protonated And Deprotonated Forms in Ethanol at B3LYP,[a] M06-2X,[a] and ωB97XD[a]**

	B3LYP/6-31G(d,p)	B3LYP[a]	M06-2X[a]	ωB97XD[a]
AH$_2^+$ (R1) → AH (R1) + H$^+$	15.84	11.25	8.23	12.47
AH$_2^+$ (R2) → AH (R2) + H$^+$	8.34	5.26	1.76	6.16
AH$_2^+$ (R3) → AH (R3) + H$^+$	11.34	18.45	4.85	9.49
AH (enol) → A$_1^-$ + H$^+$	28.90	21.30	20.44	23.17
AH (keto) → A$_1^-$ + H$^+$	26.55	19.92	16.84	21.14
AH (R1) → A$_1^-$ + H$^+$	21.97	15.50	15.51	17.78
AH (R2) → A$_2^-$ + H$^+$	18.98	13.07	13.06	15.58
AH (R3) → A$_2^-$ + H$^+$	19.84	3.15	13.72	15.99

[a]Method/6-311++G(2d,2p)// B3LYP/6-31G(d,p).

Table 9. First λ_{max} for 2OHPhAZ Using Different Functionals (Solvation Model, Acetonitrile)/6-311+G(d,p)//B3LYP/6-31G(d,p) with a Variety of Solvation Models (Experimental[26] Value Is 495 nm)[a]

model\functional	B3LYP	CAM-B3YP	PBE	PBE[b]	ωB97X-D	M06-2X	CIS
CPCM	448 (0.2715)	423 (0.2067)	513 (0.2005)	514 (0.2005)	422 (0.1906)	422 (0.2048)	361 (0.5763)
SMD	445 (0.2765)	420 (0.2166)	506 (0.2131)	508 (0.2125)[c]	418 (0.2003)	419 (0.2143)	360 (0.6115)
PCM	447 (0.2626)	422 (0.1992)	512 (0.1934)	513 (0.1933)	421 (0.1836)	421 (0.1973)	358 (0.5405)
gas phase	459 (0.2169)	429 (0.1523)	553 (0.1051)	552 (0.1054)	429 (0.137)	428 (0.1513)	386 (0.2389)

[a]Values in parentheses represent oscillator strength. [b]PBE/6-311+G(2d,2p). [c]The result of PBE0/6-311+G(2d,2p) using the SMD model is 436 nm (0.2739).
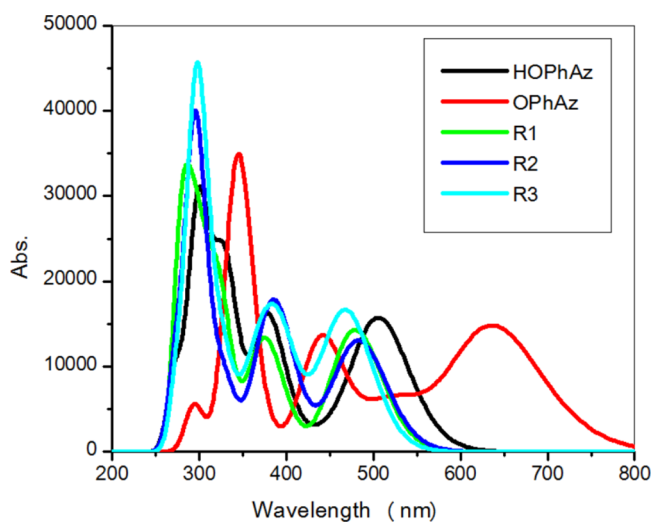
Figure 6. Simulated UV/Vis absorption spectra for the keto, enol, and rotamers of **2OHPhAZ** at TD-PBE/6−311 + G(d,p).

of the **2OPhAZ** has the highest chemical shift (19.40 ppm) that accompanies the formation of strong LBHB (N$_1$−H$_1$···O$_1$), followed by H$_1$ of the **2OHPhAZ** (14.76 ppm). On contrary, H$_1$ of the studied rotamers have lower chemical shift that range from 4 to 6 ppm. The calculated ^{1}H NMR chemical shifts for LBHB reveal an agreement, to some extent, with those reported by Hibbert and Emsley[97] for a proton chemical shift. Therefore, the calculated ^{1}H NMR chemical shifts help in confirming the presence of IHB and distinguish LBHB in the studied tautomers.

3.4. Aromaticity. Aromaticity can be assessed through energy, structural, or magnetic and reactivity criteria. One of the widely used criteria to determine the aromaticity of the studied compound is nucleus-independent chemical shifts (NICS), which is a magnetic-based criterion.[34,98,99] NICS is defined as the negative of the absolute magnetic shielding calculated at selected points near the investigated molecule

starting from zero to a couple of angstroms, in the ring center, above it or sometimes on grids. Negative NICS values imply diatropic ring current that reflects aromatic character, and positive ones indicate paratropic ring current, which leads to antiaromaticity, while zero NICS means nonaromatic. Although the NICS index is somewhat sensitive to basis set, previous studies[34,100] calculated NICS as single point at B3LYP/6-31G(d,p) with a reasonable accuracy. NICS(0) refers to the isotropic shielding at the center of the ring, while NICS(1) is computed at 1 Å above the ring center. However, NICS(0)$_{zz}$ and NICS(1)$_{zz}$ correspond to the out-of-plane component of the magnetic shielding tensor. Among the four NICS indices, the NICS(1)$_{zz}$ will be used in further discussion because it gives a reliable measure of magnetic shielding of the out-of-plane component of NICS[99,101−105] and correlates well with π-electron delocalization and the ring current.[103−105] Because NICS is not sufficient to predict the antiaromaticity of the heteroaromatic system,[104−107] another criterion has been used to determine aromaticity such as the geometrical-based HOMA.[35−37] The higher the HOMA value, the more aromatic is the ring in question, and hence, more delocalized the π electrons of the calculated ring. It is defined as follows:

$$\text{HOMA} = 1 - \frac{1}{n}\sum_{j=1}^{n}\alpha_i(R_{\text{opt},i} - R_j)^2 \tag{11}$$

where n represents the total number of bonds in the molecule, and α_i is a normalization constant (α_{CC} = 257.7 and α_{CN} = 93.52). R_{opt} is the optimized bond length, for C−C = 1.388 Å and for C−N bond R_{opt} = 1.334 Å. It is worth noting that the HOMA is a relative index and that the maximum aromaticity is found when HOMA = 1 and it equals zero for a nonaromatic system.[108]

For the investigated systems, NICS$_{zz}$ and HOMA calculations were performed at the B3LYP/6-31G(d,p) level in the gas and ethanol to evaluate the aromatic character of each ring are presented in Table 4. Apparently, the NICS and HOMA

Table 10. Excitation Energies (eV) at (TD-PBE-SMD, Acetonitrile)/6-311 + G(d,p)//B3LYP/6-31G(d,p), Oscillator Strengths ($f > 0.15$), and their Transition Characters for 2OHPhAZ Tautomer and Rotamers

compound	state	E^a	f	assignment[b]
2OHPhAZ	1	2.45 (506)	0.2131	H → L (88%)
	4	3.28 (378)	0.2137	H−2 → L (55%), H−1 → L+1 (27%), H → L+1 (11%)
	6	3.76 (329)	0.2990	H−2 → L (10%), H−2 → L+1 (27%), H−1 → L + 1 (40%), H → L+1 (12%)
	8	4.18 (297)	0.2947	H−4 → L (27%), H−2 → L+1 (45%), H−1 → L + 1 (13%), H → L+2 (10%)
2OPhAZ	1	1.94 (638)	0.2023	H → L (89%)
	4	2.81 (441)	0.1868	H−2 → L (90%)
	7	3.59 (346)	0.4396	H−3 → L (40%), H−2 → L+1 (34%), H → L+2 (14%)
R1	1	2.59 (479)	0.1951	H → L (88%)
	6	3.84 (323)	0.2506	H−4 → L (15%), H-2 → L+1 (31%), H-1 → L+1 (26%), H → L+1 (17%)
	9	4.17 (297)	0.2348	H−3 → L + 1 (13%), H−2 → L +1 (16%), H → L+2 (50%)
	10	4.43 (280)	0.3647	H−1 → L+2 (70%)
R2	1	2.56 (483)	0.1759	H → L (86%), H−2 → L (11%)
	8	4.20 (295)	0.3645	H−3 → L+1 (24%), H → L+2 (53%)
	10	4.54 (273)	0.1509	H−1 → L+2 (82%)
R3	1	2.63 (471)	0.2036	H−2 → L (11%), H → L (84%)
	3	3.15 (393)	0.1745	H−2 → L (65%), H → L+1 (21%)
	6	3.81 (325)	0.1594	H−2 → L+1 (60%), H−1 → L +1 (11%), H → L+1 (15%)
	8	4.18 (297)	0.4859	H−1 → L+1 (11%), H → L+2 (66%)

^{a}Values in parentheses are wave lengths in nm. ^{b}Only contributions above 10% are shown. H and L represent HOMO and LUMO, respectively.

results in Table 4 provide a good match with previous studies on benzene,[109] pyrrole,[110] $C_7H_7^+$,[111] azulene,[34,112,113] and azaazulene[114] and also can support the order of stability. Both $NICS(1)_{zz}$ and HOMA indices show good performance with the relative energies of enol and keto tautomers. The phenyl ring of **2OHPhAZ** has a high value of HOMA (0.89) and a negative value of $NICS(1)_{zz}$ (−18.66 ppm) than **2OPhAZ** ($NICS(1)_{zz}$/HOMA; −12.01/0.51) in the gas phase as its aromaticity does not affect the delocalization in the RAHB. The lower values of HOMA of the five-membered ring in the enol form **2OHPhAZ** compared to keto tautomer **2OPhAZ** point out to the participation of its electron delocalization to the IHB ring and, therefore, increase RAHB in the enol form. The seven-membered ring for all the studied structures has a higher HOMA value than the five-membered one, indicating their higher aromatic character. Very negligible changes of magnetic indices of aromaticity are observed upon the presence of the polar solvent, like water or chloroform. π-electron delocalization of the phenyl ring in the studied rotamers has a slightly higher aromaticity than that in the enol

and keto forms. This picture is in line with other observations.[84,115]

The stability and aromaticity are related concepts, and thus, some of the DFT descriptors can be discussed to analyze aromaticity.[116−120] Table 5 lists the energies of the HOMO, the LUMO, energy gap (E_g), vertical IP, and EA as well as η, S, χ, μ, and ω. From Table 5, it has been found that the keto form has the lowest HOMO−LUMO gap (2.30 eV) followed by enol forms (3.08 eV). The rotamers have the highest energy gap (3.35−3.47 eV). It is known that the lower the energy gaps, the higher the reactivity of the molecule.[121,122] Thus, the keto form is expected to have high chemical reactivity, low hardness, high softness, and highest electrophilicity than enol and their rotamers. This might explain the low aromaticity of the keto form and its high global activity. In accordance with the summation of the calculated NICS and HOMA indices presented in Table 4, the enol and rotamers forms illustrate lower electrophilicity (ω) and higher hardness (η) than the keto form, which reflects high aromatic character of the former structures.

3.5. Charge Distribution, Fukui Functions, and ESP Analysis. The charge distribution and the ESP surface are widely used to determine the reactivity of a given molecule and its expected interaction with other systems. NPA charges of some selected atoms of the investigated structures have been calculated in the gas phase at the B3LYP/6-31G(d,p) level (Table 6). For **2OHPhAZ** tautomers and rotamers. The results indicate high negative charges on the N1 and O1 atoms and high positive charge on H1. The highest negative and positive charges on the O (−0.701 e), N (−0.557 e), and H (0.522 e) atoms for the enol form indicate the larger electrostatic interaction through N···H−O IHB. The high negative charge on the O and N atoms of enol sheds light on the potential use of this structure as a bidentate ligand when they come close to metal ions.

The calculated condensed Fukui functions (f_k^+, f_k^-, and f_k^0) evaluated from NPA for the investigated tautomer and rotamers at B3LYP/6-31G(d,p) are given in Tables 7 and S5. Higher values indicate more reactivity.[123,124] An inspection of these data reveals that the preferred site for electrophilic attack for **2OHPhAZ** and **2OPhAZ** tautomers are C6, and for **R1, R2 and R3** are C7 and C5 of the highest value of f^-. On the other hand, H1 and C6 (**2OHPhAZ, 2OPhAZ and R1**) are the sites prone to nucleophilic attack as they have the highest f^+ values. Table 7 shows that at the DFT level, the most susceptible site to a nucleophilic attack for **R2** is located on O1 and C3′. For Rotamer **R3**, the reactivity descriptors show that H1 and C3′ are more reactive site for nucleophilic attack. For **2OHPhAZ, 2OPhAZ, R1** (H1, C6), **R2** (C6, C5′), and **R3** (O1, C3′) are the most active site for free radical reactions.

The charged regions in the molecule can be depicted by ESP maps. The different colors represent different values of the electrostatic potential. The potential increases in the order red < orange < yellow < green < blue. The red color in ESP maps represents the most negative electrostatic potential while the blue color reflects the most positive electrostatic potential regions. The ESP surfaces of investigated structures obtained using B3LYP/6-31G(d,p) are depicted in Figure 4. ESP of enol/keto forms shows the localization of a significant negative charge on the O atom while blue color appears around some hydrogen atoms of the azaazulene ring. Therefore, the O atom has the ability for electron donation to electron-deficient centers such as metal ions. A slight electron-donating ability of
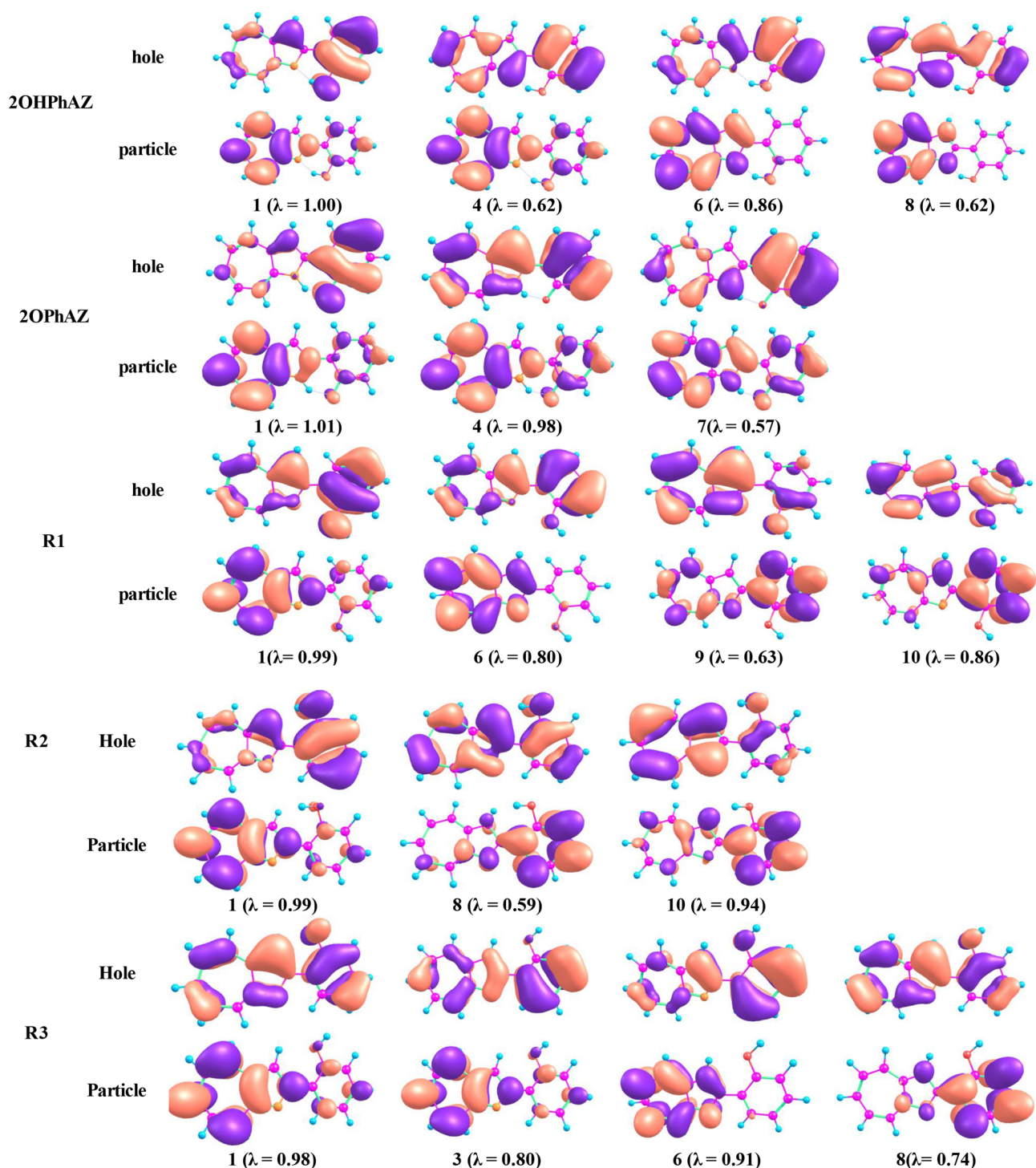
Figure 7. NTOs for the excitation with significant and small but non-negligible oscillation strengths for the studied structures at the PBE/6-311+G(d,p) level with solvent effects of acetonitrile through SMD. The displayed occupied (holes) and unoccupied (electrons) NTO pairs are only that have contribution more than 50% to each excited state (λ is eigenvalues of the pairs).

the N atom has been noticed as well. A remarkable blue color on the H1 attached to O atoms in rotamers has been observed where there is no nearby nitrogen (**R1** and **R3**) or C═C bonds (**R2**). A clear electron-rich area (red color) has been observed in the region between N1 and O1 atoms in **R1**, which denotes a bidonating ability of this compound when interacting with metal ions as reported experimentally for similar azaazulene derivatives.[23−26]

3.6. Acidity and Basicity. Our investigated compound has one labile proton which is attached to either a nitrogen or oxygen atom. The reliable and quick estimation of the acidity and basicity of a molecule without synthesis and experimental determination is very important to interpret the structure reactivity and property relationships. Moreover, knowledge of the acidity constants, (pK_a), is important for determining equilibrium constant (K) of reactions, especially that involving proton transfers. However, when the determination of pK_a

experimentally is difficult, computational approaches can be applied to estimate the pK_a using the thermodynamic free energies cycle that is shown in Scheme 3. Consequently, DFT calculations were applied to study the possible protonated (cation) and deprotonated (anion) forms of 2-(2-hydroxyphenyl)-1-azaazulene that is depicted in Figure 5. The protonated form, denoted as AH_2^+, has a net charge of +1, while the corresponding enol/rotamers or keto, AH, is neutral. According to the optimized structure of the protonated form, the hydroxyl group of the phenyl ring has been rotated to give the rotamer structure. Therefore, throughout the acidity constant calculation from the protonated form, we will consider the energy of the rotamer. On the other hand, the deprotonated form, denoted as A^-, has a net charge of −1. The equations used for calculating pK_a values are given below:

$$pK_a = \Delta G_{AH_2^+}(aq)/2.303RT \qquad (12)$$

$$\Delta G_{AH_2^+}(aq) = \Delta G_{AH_2^+}(g) + \Delta\Delta G_{AH_2^+}(solv) \qquad (13)$$

$$\Delta G_{AH_2^+}(g) = G_{AH}(g) + G_{H^+}(g) - G_{AH_2^+}(g) \qquad (14)$$

$$\Delta\Delta G_{AH_2^+}(solv) = \Delta G_{AH}(solv) + \Delta G_{H^+}(solv) - \Delta G_{AH_2^+}(solv) \qquad (15)$$

where $G_i(g)$ is the standard free energy of the species "i" in the gas phase, $\Delta G_i(solv)$ is the solvation free energy of "i", and $G_i(aq)$ is the free energy change in the aqueous phase. The $G_{H^+}(g)$ and $\Delta G_{H^+}(solv)$ values are −6.28[125,126] and − 265.90 kcal/mol,[127,128] respectively.

The experimental acidity constants were taken in our consideration. The correlation between the experimental and the calculated acidity constants revealed that the ωB97XD/6-311++G(2d,2p) level yields the closest pK_a value to experiment. As given in Table 8, the experimental pK_a of **2OHPhAZ** was reported as 12.7,[26] and the calculated pK_a from the protonated form is found as 15.84, 11.25, 8.23, and 12.47 using B3LYP/6-31G(d,p), B3LYP/6-311++G(2d,2p), M06-2X/6-311++G(2d,2p), and ωB97XD/6-311++G(2d,2p) levels, respectively. By comparing the pK_a obtained by deprotonation, we can find that the enol form is a weaker acid than its keto and rotamers. This can be attributed to the strength of the OH and NH bonds, presence or absence of hydrogen bonds, and the stability of the resulting conjugate base upon deprotonation. More negative charges on the nitrogen and oxygen atoms for enol than keto and rotamers forms (Table 6) might reflect the strength of the OH and NH bonds.

In this study, we examine the intrinsic basicity in the gas phase that can be given by proton affinity (PA), which is the negative of the protonation reaction of AH.

$$AH + H^+ \rightarrow AH_2^+, \quad PA = -\Delta H^\circ \qquad (16)$$
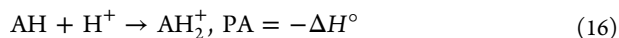
According to a previous study on the 2-pyridone tautomer and rotamer,[73] Michelson et al. found that the stable enol form has lower PA followed by the keto form with difference 5.7 kcal/mol at M06-2X/6-311 + G(2df,2p), and the rotamer has slightly higher PA. Our calculated PA of 2-(2-hydroxyphenyl)-1-azaazulene tautomer differs by 8.6 kcal/mol (241.88 (enol) versus 250.51 (keto), kcal/mol), while the rotamer forms are slightly higher in the calculated PA than the enol form (254.92, 242.81, and 248.13 kcal/mol for **R1**, **R2**, and **R3**, respectively) at ωB97XD/6-311++G(2d,2p). The calculated PA at B3LYP/6-31G(d,p), B3LYP/6-311++G(2d,2p), M06-2X/6-311++G-

(2d,2p), and ωB97XD/6-311++G(2d,2p) levels has been listed in Table S6.

3.7. UV−Vis Spectral Analysis. Potential use of any compound as a dye or sensor can be deduced from its photophysics and photochemistry. The first maximum wavelength of absorption using TDDFT calculation of the **2OHPhAZ** in the gas phase by means of different solvation models PCM, CPCM, and SMD at different levels of theory such as B3LYP, CAM-B3LYP, PBE,PBE0, ωb97X-D, M06-2X, and CIS with the 6-311+G(d,p) basis sets is collected in Table 9. The results of calculations are compared with the available experimental data. The TDDFT-PBE/SMD model chemistry exhibits a good quantitative agreement regarding the first and second maximum excitation peak (E_{ex}; the discrepancy between the calculated and experimental first maximum and second excitation energy 11 and 12 nm, respectively).[26]

The hydrogen bond is one of the reasons responsible for the strength, broadening, and shift of the absorption peaks. Table 9 presents the values of E_{ex}, oscillator strength f, and transition configurations of the intense peaks for enol, keto, and rotamers. The keto form with the short HB is accompanied by a large redshift (extended to 800 nm) followed by the enol form (extended to 650 nm), and the lower shift has been found with the rotamers (extended to 550 nm), as depicted in Figure 6. As expected from the lower E_g value of the keto, enol, and rotamers (Table 5), the maxima in the electronic absorption spectra of keto in comparison with enol, **R1**, **R2**, and **R3** are shifted bathochromically by 17, 66, 51, and 49 nm, respectively. The intense peaks in the UV−vis spectra of keto spread over the range of 346−638 nm followed by enol that illustrates spreading over the range 272−506 nm, and the their rotamers (**R1**, **R2**, and **R3**) peaks spread over the range (280−479, 273−483, and 276−471 nm, respectively). The strong electronic absorption of keto is attributed to the HOMO−3 to LUMO and HOMO−2 to LUMO+1 transitions. The maximum absorption peak for enol appears at a lower wavelength than keto, which is attributed to HOMO−2 to LUMO+1 and HOMO−1 to LUMO+1 transitions. However, the strong electronic absorption of the rotamer **R1** is mainly due to the HOMO−1 to LUMO+2 transitions. The strong electronic absorption of the studied rotamers has different contribution, as shown in Table 10.

The NTOs for high-intensity excited states of the investigated systems are shown in Figure 7 to analyze the nature of absorption. The occupied and unoccupied NTOs are referred to as "hole" and "particles" transition orbitals, respectively. The NTOs generally give a simpler description of the excited state than the canonical orbitals. As displayed in Figure S4, where the canonical orbitals were used, the dominant transitions are $\pi-\pi*$ for the excitations with some contribution from n−$\pi*$ excitation. This makes the analysis of excitations cumbersome. However, as depicted in Figure 7, the hole NTOs contributing to the illustrated band shown in Figure 6 and Table 10 of all studied structures are delocalized over the whole molecular skeleton while the particles NTOs are mainly delocalized over either azaazulene or benzene rings. This suggests $\pi-\pi*$ excitation.

4. CONCLUSIONS

Tautomer and the related rotamers of 2-(2-hydroxyphenyl)-1-azaazulene (**2OHPhAZ**) were theoretically investigated for analyzing various molecular properties, stability, and aromaticity. Relative energy results reveal that M06-2X/6-311+

+G(2d,2p) has a good performance compared to CCSD(T)/6-311++G(2d,2p). The structural parameters and vibrational frequencies have been discussed at B3LYP/6-31G(d,p) and compared with the available experimental data. Comparisons with the experiment of 2-(2-hydroxyphenyl)-1-azaazulene show a very good agreement. All the levels of calculations demonstrate thermodynamic and kinetic stability of the enol form in a good agreement with the presence of enol experimentally exclusively as the most stable tautomer. The remarkable chemical shift of a proton at 14.76 and 19.40 ppm in the nuclear magnetic resonance spectrum has been attributed to the existence of LBHBs for the enol and keto forms, respectively. The aromaticity of the enol and rotamers forms is slightly higher than the keto form. Hardness and the electrophilicity trend show a good correlation with the HOMA and NICS aromaticity indices. The sites of electrophilic and nucleophilic were determined using Fukui functions. UV–vis absorption spectra (in the gas phase and ethanol) were examined by TD-DFT using B3LYP, CAM-B3LYP, PBE, PBE0, ωb97X-D, M06-2X, and CIS methods with the 6–311+G(d,p) basis sets for **2OHPhAZ**. The TDDFT-PBE/SMD approaches exhibit good agreement regarding the first and second maximum excitation peaks. NTOs are used to indicate the $\pi-\pi^*$ nature of the transitions.

■ ASSOCIATED CONTENT

Ⓢ Supporting Information

The Supporting Information is available free of charge at https://pubs.acs.org/doi/10.1021/acsomega.2c00866.

> Supplementary data associated with this article can be found in the online version. Figure S1: Optimized structures of interconversions of keto-enol tautomers and rotamers (**TS$_T$**, **TS$_R$**) of 2-(2-Hydroxyphenyl)-1-azaazulene (2OHPhAZ) at B3LYP/6-31G(d,p). Figure S2: Potential energy profiles from the IRC calculation for tautomerization and rotamerization of 2OHPhAZ obtained at the B3LYP/6-31G (d, p) level. Figure S3: Change of bond lengths (angstroms) along reaction coordinates for tautomarization of 2OHPhAZ at the B3LYP/6-31G(d,p) level. Figure S4: Frontier orbitals of the studied structures at B3LYP/6-31G(d,p). Table S1: Root-mean-square atom positional deviations (RMSD) values, in Å, calculated for the studied system on the calculated structure of enol (**2OHPhAZ**) in the gas phase. Table S2: dihedral angle in the degree of N1–C2–C1′–C2′, C2–C1′–C2′–O1 and C1′–C2′–O1–H1 for **R1**, **R2**, and **R3** with their corresponding TSs. Table S3: Relative Gibbs free energies (ΔG_{298}) and Gibbs Free Energy Barrier ($\Delta G_{298}^{\ddagger}$) for the tautomer and rotamers forms of 2OHPhAZ in kcal/mol, in the gas-phase and under the effect of ethanol calculated at the B3LYP/6-31G(d,p), B3LYP/6-311++G(2d,2p) and ωB97XD/6-311++G(2d,2p) levels of theory. Table S4: ^{13}C and ^{1}H NMR chemical shifts (in ppm) calculated at the B3LYP/6-31G(d,p) level of theory for the 2OHPhAZ tautomer and rotamers using the GIAO method in CHCl$_3$. Table S5: Condensed Fukui functions (f_k^+, f_k^-, f_k^0) of the hydrogen: atoms[a] for the investigated tautomer and rotamers at B3LYP/6-31G-(d,p). Table S6: Calculate proton affinity (PA) for 2OHPhAZ tautomers and rotamers in the gas phase at B3LYP, M06-2X, and ωB97XD (PDF)

■ AUTHOR INFORMATION

Corresponding Authors

Safinaz H. El-Demerdash − *Chemistry Department, Faculty of Science, Menoufia University, Shebin El-Kom 32512, Egypt;* ⊙ orcid.org/0000-0002-9733-3666; Email: hamdysafinaz@yahoo.com

Ahmed M. El-Nahas − *Chemistry Department, Faculty of Science, Menoufia University, Shebin El-Kom 32512, Egypt;* ⊙ orcid.org/0000-0002-8547-7574; Email: amelnahas@hotmail.com

Authors

Asmaa B. El-Meligy − *Chemistry Department, Faculty of Science, Menoufia University, Shebin El-Kom 32512, Egypt*

Mohamed A. Abdel-Rahman − *Chemistry Department, Faculty of Science, Suez University, Suez 41522, Egypt;* ⊙ orcid.org/0000-0002-9895-3584

Mohamed A. M. Mahmoud − *Basic Sciences Department, Tanta Higher Institute of Engineering and Technology, Tanta 31511, Egypt*

Tetsuya Taketsugu − *Department of Chemistry, Faculty of Science, Hokkaido University, Sapporo 060-0810, Japan; Institute for Chemical Reaction Design and Discovery (WPI-ICReDD), Hokkaido University, Sapporo 060-0810, Japan;* ⊙ orcid.org/0000-0002-1337-6694

Complete contact information is available at:
https://pubs.acs.org/10.1021/acsomega.2c00866

Author Contributions

A.B.E.: conceptualization, methodology, formal analysis, data curation, validation, visualization, and investigation, and writing-review and editing, S.H.E.: conceptualization, methodology, formal analysis, data curation, validation, visualization, investigation, and writing—review and editing. M.A.A.: conceptualization, methodology, formal analysis, data curation, validation, visualization, investigation, and writing—review and editing, M.A.M.M.: conceptualization, methodology, formal analysis, data curation, validation, visualization, investigation, and writing-review and editing. T.T.: formal analysis, data curation, validation, and writing—review and editing. A.M.E.: formal analysis, data curation, validation, visualization, investigation, supervision, and writing—review and editing. All authors read and approved the final manuscript.

Notes

■ REFERENCES

(1) Anderson, A. G.; Nelson, J. J. A. Electrophilic Substitution Of Azulene. *J. Am. Chem. Soc.* **1950**, *72*, 3824−3825.

(2) Buenker, R. J.; Peyerimhoff, S. D. Ab Initio SCF Calculations for Azulene and Naphthalene. *Chem. Phys. Lett.* **1969**, *3*, 37−42.

(3) Liu, R. S. H. Colorful Azulene and Its Equally Colorful Derivatives. *J. Chem. Educ.* **2002**, *79*, 183−185.

(4) Lemal, D. M.; Goldman, G. D. Synthesis of Azulene, a Blue Hydrocarbon. *J. Chem. Educ.* **1988**, *65*, 923−925.

(5) Mikheev, Y. A.; Guseva, L. N.; Ershov, Y. A. The Structure of Dimers and the Nature of Azulene Chromaticity. *Russ. J. Phys. Chem. A* **2012**, *86*, 85−92.

(6) Murakami, A.; Kobayashi, T.; Goldberg, A.; Nakamura, S.; Murakami, A.; Kobayashi, T.; Goldberg, A.; Nakamura, S. CASSCF and CASPT2 Studies on the Structures , Transition Energies, and

Dipole Moments of Ground and Excited States for Azulene. *J. Chem. Phys.* **2004**, *120*, 1245−1252.

(7) Pariser, R. Electronic Spectrum and Structure of Azulene. *J. Chem. Phys.* **1956**, *25*, 1112−1116.

(8) Birks, J. B. The Photophysics of Azulene. *Chem. Phys. Lett.* **1972**, *17*, 370−372.

(9) Liu, R. S. H.; Asato, A. E. Tuning the Color and Excited State Properties of the Azulenic Chromophore: NIR Absorbing Pigments and Materials. 2003, 4, 179−194, DOI: 10.1016/j.jphotochemrev.2003.09.001.

(10) Rekka, E.; CHrysselis, M.; Siskou, I.; Ourounakis, A. K. Synthesis of New Azulene Derivatives and Study of Their Effect on Lipid Peroxidation and Lipoxygenase Activity. *Chem. Pharm. Bull.* **2002**, *50*, 904−907.

(11) Wang, B.; Lin, Y.; Chang, J.; Wang, P. Theoretical Studies of Azulene and Its Derivatives. *Can. J. Chem.* **2000**, *78*, 224−232.

(12) El-Nahas, A. M.; Staykov, A.; Yoshizawa, K. First-Principles Calculations of Electron Transport through Azulene. *J. Phys. Chem. C* **2016**, *120*, 9043−9052.

(13) Haidar, E.; Tawfik, S. A.; Stampfl, C.; Hirao, K.; Yoshizawa, K.; Nakajima, T.; Soliman, K. A.; El-Nahas, A. M. Attenuation of Redox Switching and Rectification in Azulenequinones/Hydroquinones after B and N Doping: A First-Principles Investigation. *Adv. Theory Simul.* **2020**, *4*, No. 2000203.

(14) El-Nahas, A. M.; Staykov, A.; Yoshizawa, K. Electrical Conductivity and Diode-Like Behavior of Substituted Azulene Electrical Conductivity and Diode-Like Behavior of Substituted Azulene. *J. Phys. Chem. C* **2017**, *121*, 2504−2511.

(15) Haidar, E.-A.; Tawfik, S. A.; Stampfl, C.; Hirao, K.; Yoshizawa, K.; El-Demerdash, S. H.; Nakajima, T.; El-Nahas, A. M. Electronic Transport Investigation of Redox-Switching of Azulenequinones/Hydroquinones via First-Principles Studies. *Phys. Chem. Chem. Phys.* **2019**, *21*, 17859−17867.

(16) Gad, S. F.; El-Demerdash, S. H.; El-Mehasseb, I. M.; El-Nahas, A. M. Structure, Stability and Conversions of Tautomers and Rotamers of Azulene-Based Uracil Analogue. *J. Mol. Struct.* **2019**, *1182*, 271−282.

(17) Meshhal, M. M.; El-Demerdash, S. H.; El-Nahas, A. M. A Thermochemical Computational Study on Hydroxyquinolines and Their Azulene Analogues. *J. Mol. Struct.* **2019**, *1183*, 70−77.

(18) Ramadan, M.; Goeters, S.; Watzer, B.; Krause, E.; Lohmann, K.; Bauer, R.; Hempel, B.; Imming, P.; Chemie, P.; Philipps-uni, V.; Jugendmedizin, K.; Philipps-uni, V.; Biologie, P.; Heinrich-heine-uni, V.; Wissenschaften, P.; Karl-franzens-uni, V.; Gmbh, R.; Pharmazie, F.; Martin-luther-uni, V. Chamazulene Carboxylic Acid and Matricin: A Natural Profen and Its Natural Prodrug, Identified through Similarity to Synthetic Drug Substances. *J. Nat. Prod.* **2006**, *69*, 1041−1045.

(19) Ishihara, M.; Wakabayashi, H.; Motohashi, N.; Sakagami, H. Quantitative Structure−Cytotoxicity Relationship of Newly Synthesised Trihaloacetylazulenes Determined by a Semi-Empirical Molecular-Orbital Method (PM5). *Anticancer Res.* **2011**, *31*, 515−520.

(20) Abe, N.; Gunji, T. The Chemistry of Azaazulenes. *Heterocycles* **2010**, *82*, 201−248.

(21) Kimura, M. The Chemistry of Aza-Azulenes. *J. Synth. Org. Chem., Jpn.* **1981**, *39*, 690−700.

(22) Turányi, T.; Zalotai, L.; Dóbé, S.; Bérces, T. Effect of the Uncertainty of Kinetic and Thermodynamic Data on Methane Flame Simulation Results. *Phys. Chem. Chem. Phys.* **2002**, *4*, 2568−2578.

(23) Abe, N.; Hashimoto, E.; Fujii, H.; Murakami, Y.; Tagashira, S.; Kakehi, A. Synthesis of 2-Chloro-8-(2-Pyridyl)-1-Azaazulene and Its Metal Complexes. *Heterocycles* **2004**, *63*, 2341−2348.

(24) Oda, M.; Miyawaki, D.; Matsumoto, N.; Kuroda, S. Palladium-Catalyzed Amination of 2-Chloro-1-Azaazulene with 2-Aminopyridine. *Heterocycles* **2011**, *83*, 547−554.

(25) Oda, M.; Ogura, K.; Thanh, N. C.; Kishi, S.; Kuroda, S.; Fujimori, K.; Noda, T.; Abe, N. Synthesis and Properties of 2-(2-Pyridyl)-1-Azaazulene. *Tetrahedron Lett.* **2007**, *48*, 4471−4475.

(26) Oda, M.; Sugiyama, A.; Takeuchi, R.; Fujiwara, Y.; Miyatake, R.; Abe, T.; Kuroda, S. Synthesis, Molecular Structure, and Properties of 2-(2-Hydroxyphenyl)-1- Azaazulene. *Eur. J. Org. Chem.* **2012**, *6*, 2231−2236.

(27) Philips, J. P. The Reactions of 8-Quinolinol. *Chem. Rev.* **1956**, *56*, 271−297.

(28) Casado-Sánchez, A.; Uygur, M.; González-Muñoz, D.; Aguilar-Galindo, F.; Nova-Fernández, J. L.; Arranz-Plaza, J.; Díaz-Tendero, S.; Cabrera, S.; Mancheño, O. G.; Alemán, J. 8-Mercaptoquinoline as a Ligand for Enhancing the Photocatalytic Activity of Pt(II) Coordination Complexes: Reactions and Mechanistic Insights. *J. Org. Chem.* **2019**, *2019*, 6437−6447.

(29) Vila, J. A.; Arnautova, Y. A.; Vorobjev, Y.; Scheraga, H. A. Assessing the Fractions of Tautomeric Forms of the Imidazole Ring of Histidine in Proteins as a Function of PH. *Proc. Natl. Acad. Sci. U. S. A.* **2011**, *108*, 5602−5607.

(30) Minkin, V. I.; Olekhnovich, L. P.; Zhdanov, Y. A. Molecular Design of Tautomeric Compounds. *Acc. Chem. Res.* **1981**, *3*, 210−217.

(31) Pople, J. A.; Head-Gordon, M.; Raghavachari, K. Quadratic Configuration Interaction. A General Technique for Determining Electron Correlation Energies. *J. Chem. Phys.* **1987**, *87*, 5968−5975.

(32) Purvis, G. D.; Bartlett, R. J. A Full Coupled-Cluster Singles and Doubles Model: The Inclusion of Disconnected Triples. *J. Chem. Phys.* **1982**, *76*, 1910−1918.

(33) Buhl, M.; van Wiillen, C. Computational Evidence for a New C84 Isomer. *Chem. Phys. Lett.* **1995**, *247*, 63−68.

(34) von Ragué Schleyer, P.; Maerker, C.; Dransfeld, A.; Jiao, H.; van Eikema Hommes, N. J. R. Nucleus-Independent Chemical Shifts: A Simple and Efficient Aromaticity Probe. *J. Am. Chem. Soc.* **1996**, *118*, 6317−6318.

(35) Sobczyk, L.; Grabowski, S. J.; Krygowski, T. M. Interrelation between H-Bond and Pi-Electron Delocalization. *Chem. Rev.* **2005**, *105*, 3513−3560.

(36) Krygowski, T. M. Crystallographic Studies of Inter- and Intramolecular Interactions Reflected in Aromatic Character of Pi-Electron Systems. *J. Chem. Inf. Comput. Sci.* **1993**, *33*, 70−78.

(37) Kruszewski, J.; Krygows, T. M. Definition of Aromaticity Basing on the Harmonic Oscillator Model. *Tetrahedron Lett.* **1972**, *13*, 3839−3842.

(38) Becke, A. D. A New Mixing of Hartree-Fock and Local-Density-Functional Theories. *J. Chem. Phys.* **1993**, *98*, 1372−1377.

(39) Lee, C.; Yang, W.; Parr, R. G. Development of the Colle-Salvetti Correlation-Energy Formula into a Functional of the Electron Density. *Phys. Rev. B* **1988**, *37*, 785−789.

(40) Stephens, P. J.; Devlin, F. J.; Chabalowski, C.; Frisch, M. J. Ab Initio Calculation of Vibrational Absorption and Circular Dichroism Spectra Using Density Functional Force Fields. *J. Phys. Chem.* **1994**, *98*, 11623−11627.

(41) Zhurko, G. A.; Zhurko, D. A. Chemcraft 1.8. www.chemcraftprog.com.

(42) Gonzalez, C.; Sosa, C.; Schlegel, H. B. Ab Initio Study of the Addition Reaction of the Methyl Radical to Ethylene and Formaldehyde. *J. Phys. Chem.* **1989**, *93*, 2435−2440.

(43) Gonzalez, C.; Schlegel, H. B. Reaction Path Following in Mass-Weighted Internal Coordinates. *J. Phys. Chem.* **1990**, *94*, 5523−5527.

(44) Zhao, Y.; Truhlar, D. G. The M06 Suite of Density Functionals for Main Group Thermochemistry, Thermochemical Kinetics, Noncovalent Interactions, Excited States, and Transition Elements: Two New Functionals and Systematic Testing of Four M06-Class Functionals and 12 Other Function. *Theor. Chem. Acc.* **2008**, *120*, 215−241.

(45) Zhao, Y.; Schultz, N. E.; Truhlar, D. G. Design of Density Functionals by Combining the Method of Constraint Satisfaction with Parametrization for Thermochemistry, Thermochemical Kinetics, and Noncovalent Interactions. *J. Chem. Theory Comput.* **2006**, *2*, 364−382.

(46) Chai, J. D.; Head-Gordon, M. Systematic Optimization of Long-Range Corrected Hybrid Density Functionals. *J. Chem. Phys.* **2008**, *128*, 084106−084114.

(47) Mardirossian, N.; Head-Gordon, M. Ωb97X-V: A 10-Parameter, Range-Separated Hybrid, Generalized Gradient Approximation Density Functional with Nonlocal Correlation, Designed by a Survival-of-the-Fittest Strategy. *Phys. Chem. Chem. Phys.* **2014**, *16*, 9904−9924.

(48) Lin, Y. S.; Li, G.-D.; Mao, S. P.; Chai, J. D. Long-Range Corrected Hybrid Density Functionals with Improved Dispersion Corrections. *J. Chem. Theory Comput.* **2013**, *9*, 263−272.

(49) Chai, J. D.; Head-Gordon, M. Long-Range Corrected Hybrid Density Functionals with Damped Atom-Atom Dispersion Corrections. *Phys. Chem. Chem. Phys.* **2008**, *10*, 6615−6620.

(50) Reed, A. E.; Curtiss, L. A.; Weinhold, F. Intermolecular Interactions from a Natural Bond Orbital, Donor-Acceptor Viewpoint. *Chem. Rev.* **1988**, *88*, 899−926.

(51) Reed, A. E.; Weinstock, R. B.; Weinhold, F. Natural Population Analysis. *J. Chem. Phys.* **1985**, *83*, 735−746.

(52) Glendening, E. D.; Reed, A. E.; Carpenter, J. E.; Weinhold, F. *NBO Version 3.1*; Gaussian Inc.: Pittsburgh, 2003.

(53) Marenich, A. V.; Cramer, C. J.; Truhlar, D. G. Universal Solvation Model Based on Solute Electron Density and on a Continuum Model of the Solvent Defined by the Bulk Dielectric Constant and Atomic Surface Tensions. *J. Phys. Chem. B* **2009**, *113*, 6378−6396.

(54) Frisch, M. J.; Trucks, G. W.; Schlegel, H. B.; Scuseria, G. E.; Robb, M. A.; Cheeseman, J. R.; Scalmani, G.; Barone, V.; Mennucci, B.; Petersson, G. A.; Nakatsuji, H.; Caricato, M.; Li, X.; Hratchian, H. P.; Izmaylov, A. F.; Bloino, J.; Zheng, G.; Sonnenberg, J. L.; Had, M.; Ehara, M.; Toyota, K.; Fukuda, R.; Hasegawa, J.; Ishida, M.; Nakajima, T.; Honda, Y.; Kitao, O.; Nakai, H.; Vreven, T.; Montgomery, Jr., J. A.; Peralta, J. E.; Ogliaro, F.; Bearpark, M.; Heyd, J. J.; Brothers, E.; Kudin, K. N.; Staroverov, V. N.; Kobayashi, R.; Normand, J.; Raghavachari, K.; Rendell, A.; Burant, J. C.; Iyengar, S. S.; Tomasi, J.; Cossi, M.; Rega, N.; Millam, J. M.; Klene, M.; Knox, J. E.; Cross, J. B.; Bakken, V.; Adamo, C.; Jaramillo, J.; Gomperts, R.; Stratmann, R. E.; Yazyev, O.; Austin, A. J.; Cammi, R.; Pomelli, C.; Ochterski, J. W.; Martin, R. L.; Morokuma, K.; Zakrzewski, V. G.; Voth, G. A.; Salvador, P.; Dannenberg, J. J.; Dapprich, S.; Daniels, A. D.; Farkas, O.; Foresman, J. B.; Ortiz, J. V.; Cioslowski, J.; Fox, D. J. *Gaussian 09 Revision A.1*; Gaussian Inc.: Wallingford, CT, 2009.

(55) Wolinski, K.; Hinton, J. F.; Pulay, P. Efficient Implementation of the Gauge-Independent Atomic Orbital Method for NMR Chemical Shift Calculations. *J. Am. Chem. Soc.* **1990**, *112*, 8251−8260.

(56) Wolff, S. K.; Ziegler, T. Calculation of DFT-GIAO NMR Shifts with the Inclusion of Spin-Orbit Coupling. *J. Chem. Phys.* **1998**, *109*, 895−905.

(57) Cheeseman, J. R.; Trucks, G. W.; Keith, T. A.; Frisch, M. J. A Comparison of Models for Calculating Nuclear Magnetic Resonance Shielding Tensors. *J. Chem. Phys.* **1996**, *104*, 5497−5509.

(58) Stanger, A. Nucleus-Independent Chemical Shifts (NICS): Distance Dependence and Revised Criteria for Aromaticity and Antiaromaticity. *J. Org. Chem.* **2006**, *71*, 883−893.

(59) Fallah-bagher-shaidaei, H.; Wannere, C. S. Which NICS Aromaticity Index for Planar π Rings Is Best ? *Org. Lett.* **2006**, *8*, 863−866.

(60) Lucila, L.; Martinez, L.; Mitnik, G.; Borunda, E. O. Theoretical Calculation of Uv-Vis, IR Spectra and Reactivity Properties of Tamoxifen Drug: A Methodology Comparison. *MOJ Bioorg. Org. Chem.* **2017**, *1*, 87−95.

(61) Flores, M. C.; Márquez, E. A.; Mora, J. R. Molecular Modeling Studies of Bromopyrrole Alkaloids as Potential Antimalarial Compounds: A DFT Approach. *Med. Chem. Res.* **2018**, *27*, 844−856.

(62) Mishra, V. R.; Sekar, N. Photostability of Coumarin Laser Dyes - a Mechanistic Study Using Global and Local Reactivity Descriptors. *J. Fluoresc.* **2017**, *27*, 1101−1108.

(63) Das, S.; Shedge, S. V.; Pal, S. Critical Study of the Charge Transfer Parameter for the Calculation of Interaction Energy Using the Local Hard-Soft Acid-Base Principle. *J. Phys. Chem. A* **2013**, *117*, 10933−10943.

(64) Morell, C.; Toro-labbe, A. New Dual Descriptor for Chemical Reactivity. *J. Phys. Chem. A* **2005**, *109*, 205−212.

(65) Sánchez-márquez, J.; Zorrilla, D.; Sánchez-coronilla, A.; Santos, D. M. D. L.; Navas, J.; Fernández-lorenzo, C. Introducing "UCA-FUKUI" Software: Reactivity-Index Calculations. *J. Mol. Model.* **2014**, *20*, 1−13.

(66) Chattaraj, P. K.; Maiti, B.; Sarkar, U. Philicity: A Unified Treatment of Chemical Reactivity and Selectivity Pratim. *J. Phys. Chem. A* **2003**, *107*, 4973−4975.

(67) Perdew, J. P.; Burke, K.; Ernzerhof, M. Generalized Gradient Approximation Made Simple. *Phys. Rev. Lett.* **1996**, *3*, 3865−3868.

(68) Ernzerhof, M.; Perdew, J. P. Generalized Gradient Approximation to the Angle- and System-Averaged Exchange Hole. *J. Chem. Phys.* **1998**, *109*, 3313−3320.

(69) Adamo, C.; Barone, V. Toward Reliable Density Functional Methods without Adjustable Parameters: The PBE0 Model. *J. Chem. Phys.* **1999**, *110*, 6158−6170.

(70) Jacquemin, D.; Perpe, E. A.; Scuseria, G. E.; Ciofini, I.; Adamo, C. TD-DFT Performance for the Visible Absorption Spectra of Organic Dyes: Conventional versus Long-Range Hybrids. *J. Chem. Theory Comput.* **2008**, *4*, 123−135.

(71) O'Boyle, N. M.; Tenderholt, A. L.; Langner, K. M. Cclib: A Library for Package-Independent Computational Chemistry Algorithms. *J. Comput. Chem.* **2008**, *29*, 839−845.

(72) Martin, R. L. Natural Transition Orbitals. *J. Chem. Phys.* **2003**, *118*, 4775−4777.

(73) Michelson, A. Z.; Petronico, A.; Lee, J. K. 2-Pyridone and Derivatives: Gas-Phase Acidity, Proton Affinity, Tautomer Preference, and Leaving Group Ability. *J. Org. Chem.* **2012**, *77*, 1623−1631.

(74) Walker, M.; Harvey, A. J. A.; Sen, A.; Dessent, C. E. H. Performance of M06, M06-2X, and M06-HF Density Functionals for Conformationally Flexible Anionic Clusters: M06 Functionals Perform Better than B3LYP for a Model System with Dispersion and Ionic Hydrogen-Bonding Interactions. *J. Phys. Chem. A* **2013**, *117*, 12590−12600.

(75) Hejazi, S. A.; Osman, O. I.; Alyoubi, A. O.; Aziz, S. G.; Hilal, R. H. The Thermodynamic and Kinetic Properties of 2-Hydroxypyridine/2-Pyridone Tautomerization: A Theoretical and Computational Revisit. *Int. J. Mol. Sci.* **2016**, *17*, 1893.

(76) Kaczorowska, M. A.; Kaczmarek-Kędziera, A.; Ośmiałowski, B. Tautomeric Equilibrium, Proton Affinity and Mass Spectrometry Fragmentation of Flexible Hydrogen-Bonded Precursors and Rigid N → BF 2 Fluorescent Dyes. *Sci. Rep.* **2021**, *11*, 87−100.

(77) Berenbeim, J. A.; Wong, N. G. K.; Cockett, M. C. R.; Berden, G.; Oomens, J.; Rijs, A. M.; Dessent, C. E. H. Unravelling the Keto−Enol Tautomer Dependent Photochemistry and Degradation Pathways of the Protonated UVA Filter Avobenzone. *J. Phys. Chem. A* **2020**, *124*, 2919−2930.

(78) Koehl, P. Protein Structure Similarities. *Curr. Opin. Struct. Biol.* **2001**, *11*, 348−353.

(79) Shibuya, T. Efficient Substructure RMSD Query Algorithms. *J. Comput. Biol.* **2007**, *14*, 1201−1207.

(80) Kabsch, W. A Solution for the Best Rotation to Relate Two Sets of Vectors. *Acta Crystallogr., Sect. A: Cryst. Phys., Diffr., Theor. Gen. Crystallogr.* **1976**, *32*, 922−923.

(81) Shibuya, T. Searching Protein Three-Dimensional Structures in Faster Than Linear Time. *J. Comput. Biol.* **2010**, *17*, 593−602.

(82) Smallwood, C. J.; Mcallister, M. A. Characterization of Low-Barrier Hydrogen Bonds . 7. Relationship between Strength and Geometry of Short-Strong Hydrogen Bonds. The Formic Acid-Formate Anion Model System. An Ab Initio and DFT Investigation. *J. Am. Chem. Soc.* **1997**, *119*, 11277−11281.

(83) Mckenzie, R. H.; Bekker, C.; Athokpam, B.; Ramesh, S. G.; Mckenzie, R. H.; Bekker, C.; Athokpam, B.; Ramesh, S. G. Effect of Quantum Nuclear Motion on Hydrogen Bonding. *J. Chem. Phys.* **2014**, *140*, 174508.

(84) Lenain, P.; Mandado, M.; Mosquera, R. A.; Bultinck, P. Interplay between Hydrogen-Bond Formation and Multicenter π -Electron Delocalization. *J. Phys. Chem. A* **2008**, *112*, 10689−10696.

(85) Cleland, W. W.; Frey, P. A.; Gerlt, J. A. The Low Barrier Hydrogen Bond in Enzymatic Catalysis. *J. Biol. Chem.* **1998**, *273*, 25529−25532.

(86) Kong, X.; Brinkmann, A.; Terskikh, V.; Wasylishen, R. E.; Bernard, G. M.; Duan, Z.; Wu, Q.; Wu, G. Proton Probability Distribution in the O ⋯ H ⋯ O Low-Barrier Hydrogen Bond: A Combined Solid-State NMR and Quantum Chemical Computational Study of Dibenzoylmethane and Curcumin. *J. Phys. Chem. B* **2016**, *120*, 11692−11704.

(87) Perrin, C. L.; Nielson, J. B. "Strong" Hydrogen Bonds in Chemistry and Biology. *Annu. Rev. Phys. Chem.* **1997**, *48*, 511−544.

(88) Gilli, P.; Bertolasi, V.; Pretto, L.; Gilli, G. The Nature of Solid-State N-H...O/O-H...N Tautomeric Competition in Resonant Systems. Intramolecular Proton Transfer in Low-Barrier Hydrogen Bonds Formed by the ...O=C-C=N-NH... ...HO-C=C-N=N... Ketohydrazone-Azoenol System.A Variable-Temperature X-Ray Cr. *J. Am. Chem. Soc.* **2002**, *124*, 13554−13567.

(89) Hammond, G. S. A Correlation of Reaction Rates. *J. Am. Chem. Soc.* **1955**, *77*, 334−338.

(90) Gilli, G.; Bellucci, F.; Ferretti, V.; Bertolasi, V. Evidence for Resonance-Assisted Hydrogen Bonding from Crystal-Structure Correlations on the Enol Form of the,& Diketone Fragment. *J. Am. Chem. Soc.* **1989**, *111*, 1023−1028.

(91) Palusiak, M.; Simon, S.; Sola, M. Interplay between Intramolecular Resonance-Assisted Hydrogen Bonding and Aromaticity in o-Hydroxyaryl Aldehydes. *J. Org. Chem.* **2006**, *71*, 5241−5248.

(92) Krygowski, T. M.; Zachara, J. E.; Moszyn, R. Theoretical Study of Changes in π-Electron Delocalization in the Analogues of an Ortho-Hydroxy Schiff Base When the Proton Is Replaced with Li+ or BeH+. *J. Chem. Inf. Model.* **2005**, *45*, 1837−1841.

(93) Garcia-Viloca, M.; Gonzalez-Lafont, A.; Lluch, M. Theoretical Study of the Low-Barrier Hydrogen Bond in the Hydrogen Maleate Anion in the Gas Phase. Comparison with Normal Hydrogen Bonds. *J. Am. Chem. Soc.* **1997**, *119*, 1081−1086.

(94) Tolstoy, P. M.; Guo, J.; Koeppe, B.; Golubev, N. S.; Denisov, G. S.; Smirnov, S. N.; Limbach, H. Geometries and Tautomerism of OHN Hydrogen Bonds in Aprotic Solution Probed by H/D Isotope Effects on 13 C NMR Chemical Shifts. *J. Phys. Chem. A* **2010**, *114*, 10775−10782.

(95) Kumar, G. A.; Mcallister, M. A. Theoretical Investigation of the Relationship between Proton NMR Chemical Shift and Hydrogen Bond Strength. *J. Org. Chem.* **1998**, *63*, 6968−6972.

(96) Garcia-Viloca, M.; Gelabert, R.; Gonzalez-Lafont, A.; Moreno, M.; Lluch, J. M. Is an Extremely Low-Field Proton Signal in the NMR Spectrum Conclusive Evidence for a Low-Barrier Hydrogen Bond? *J. Phys. Chem. A* **1997**, *101*, 8727−8733.

(97) Hibbert, F.; Emsley, J. Hydrogen Bonding and Chemical Reactivity. *J. Adv. Phys. Org. Chem.* **1990**, *26*, 255−379.

(98) von Ragué Schleyer, P.; Manoharan, M.; Wang, Z.; Kiran, B.; Jiao, H.; Puchta, R.; van Eikema Hommes, N. J. R. Dissected Nucleus-Independent Chemical Shift Analysis of π -Aromaticity and Antiaromaticity. *Org. Lett.* **2001**, *3*, 2465−2468.

(99) Corminboeuf, C.; Heine, T.; Seifert, G.; von Ragué Schleyer, P.; Webe, J. Induced Magnetic Fields in Aromatic [n]-Annulenes— Interpretation of NICS Tensor Components. *Phys. Chem. Chem. Phys.* **2004**, *6*, 273−276.

(100) Sasaki, Y.; Takase, M.; Okujima, T.; Mori, S.; Uno, H. Synthesis and Redox Properties of Pyrrole- and Azulene-Fused Azacoronene. *Org. Lett.* **2019**, *21*, 1900−1903.

(101) Lazzeretti, P. Assessment of Aromaticity via Molecular Response Properties Y. *Phys. Chem. Chem. Phys.* **2004**, *6*, 217−223.

(102) Krygowski, T. M.; Ejsmont, K.; Stepien, B. T.; Cyran, M. K.; Poater, J.; Sola, M. Relation between the Substituent Effect and Aromaticity. *J. Org. Chem.* **2004**, *69*, 6634−6640.

(103) Krygowski, T. M.; Stepien, B. T.; Cyranski, M. K.; Ejsmont, K. Relation between Resonance Energy and Substituentresonance Effect in P-Phenols. *Phys. Org. Chem.* **2005**, *18*, 886−891.

(104) Inostroza, D.; García, V.; Yanez, O.; Torres-vega, J. J.; Vasquez-Espinal, A.; Pino-rios, R.; Báez-Grez, R.; Tiznado, W. On the NICS Limitations to Predict Local and Global Current Pathways in Polycyclic Systems. *New J. Chem.* **2021**, *45*, 8345−8351.

(105) Báez-Grez, R.; Rabanal-León, W. A.; Alvarez-Thon, L.; Ruiz, L.; Tiznado, W.; Pino-Rios, R. Aromaticity in Heterocyclic Analogues of Benzene: Dissected NICS and Current Density Analysis. *J. Phys. Org. Chem.* **2019**, *32*, 1−7.

(106) Seal, P.; Chakrabarti, S. Is Nucleus-Independent Chemical Shift Scan a Reliable Aromaticity Index for Planar Heteroatomic Ring Systems? *J. Phys. Chem. A* **2007**, *111*, 9988−9994.

(107) Foroutan-Nejad, C. Is NICS a Reliable Aromaticity Index for Transition Metal Clusters ? *Theor. Chem. Acc.* **2015**, *134*, 1−9.

(108) Mrozek, A.; Karolak-Wojciechowska, J.; Amiel, P.; Barbe, J. Five-Membered Heterocycles. Part I. Application of the HOMA Index to 1, 2,4-Trizoles. *J. Mol. Struct.* **2000**, *524*, 151−157.

(109) Dominikowska, J.; Palusiak, M. EL: The New Aromaticity Measure Based on One-Electron Density Function. *Struct. Chem.* **2012**, *23*, 1173−1183.

(110) Frizzo, C. P.; Martins, M. A. P. Aromaticity in Heterocycles : New HOMA Index Parametrization. *Struct. Chem.* **2012**, *23*, 375−380.

(111) Corminboeuf, C.; Heine, T.; Webera, J. Evaluation of Aromaticity: A New Dissected NICS Model Based on Canonical Orbitals. *Phys. Chem. Chem. Phys.* **2003**, *5*, 246−251.

(112) Meshhal, M. M.; Shibl, M. F.; El-Demerdash, S. H.; El-Nahas, A. M. A Computational Study on Molecular Structure and Stability of Tautomers of Dipyrrole-Based Phenanthroline Analogue. *Comput. Theor. Chem.* **2018**, *1145*, 6−14.

(113) Novak, I. Distorted Naphthalenes and Azulenes. *Comput. Theor. Chem.* **2017**, *1117*, 251−257.

(114) Gümüş, S. A Computational Study on Azaazulenes. *Heterocycl. Commun.* **2013**, *19*, 369−373.

(115) Cyranski, M. K.; Krygowski, T. M.; Wisiorowski, M.; van Eikema Hommes, N. J. R.; von Ragué Schleyer, P. Global and Local Aromaticity in Porphyrins: An Analysis Based on Molecular Geometries and Nucleus Independent Chemical Shift. *Angew. Chem., Int. Ed.* **1998**, *37*, 177−180.

(116) Chamizo, J. A.; Morgado, J.; Sosa, P. Organometallic Aromaticity. *Organometallics* **1993**, *12*, 5005−5007.

(117) Roy, D. R.; Bultinck, P.; Subramanian, V.; Chattaraj, P. K. Bonding , Reactivity and Aromaticity in the Light of the Multicenter Indices. *J. Mol. Struct. THEOCHEMM* **2008**, *854*, 35−39.

(118) De Proft, F.; Geerlings, P. Relative Hardness as a Measure of Aromaticity. *Phys. Chem. Chem. Phys.* **2004**, *6*, 242−248.

(119) Pausescu, I.; Medeleanu, M.; Stefanescu, M.; Peter, F.; Pop, R. A DFT Study on the Stability and Aromaticity of Heterobenzenes Containing Group 15 Elements. *Heteroat. Chem.* **2015**, *36*, 206−214.

(120) De Proft, F.; Geerlings, P. Conceptual and Computational DFT in the Study of Aromaticity. *Chem. Rev.* **2001**, *2001*, 1451−1464.

(121) Cai, T.; Xu, L.; Anderson, M. R.; Ge, Z.; Zuo, T.; Wang, X.; Olmstead, M. M.; Balch, A. L.; Gibson, H. W.; Dorn, H. C. Structure and Enhanced Reactivity Rates of the D5h Sc3N@C80 and Lu3N@C80 Metallofullerene Isomers : The Importance of the Pyracylene Motif. *J. Am. Chem. Soc.* **2006**, *128*, 8581−8589.

(122) Chermette, H. Chemical Reactivity Indexes in Density Functional Theory. *J. Comput. Chem.* **1999**, *20*, 129−154.

(123) Feng, L.; Yang, H.; Wang, F. Experimental and Theoretical Studies for Corrosion Inhibition of Carbon Steel by Imidazoline Derivative in 5% NaCl Saturated Ca (OH)2 Solution. *Electrochim. Acta* **2011**, *58*, 427−436.

(124) Rameshkumar, S.; Danaee, I.; Rashvandavei, M.; Vijayan, M. Quantum Chemical and Experimental Investigations on Equipotent Effects of (+)R and (−)S Enantiomers of Racemic Amisulpride as Eco-Friendly Corrosion Inhibitors for Mild Steel in Acidic Solution. *J. Mol. Liq.* **2015**, *212*, 168−186.

(125) Topol, I. A.; Tawa, G. J.; Burt, S. K.; Rashin, A. A. On the Structure and Thermodynamics of Solvated Monoatomic Ions Using a Hybrid Solvation Model. *J. Chem. Phys.* **1999**, *111*, 10998−11014.

(126) Jang, Y. H.; Sowers, L. C.; Çaǧin, T.; Goddard, W. A. First Principles Calculation of PKa Values for 5-Substituted Uracils. *J. Phys. Chem. A* **2001**, *2001*, 274−280.

(127) Tissandier, M. D.; Cowen, K. A.; Feng, W. Y.; Gundlach, E.; Cohen, M. H.; Earhart, A. D.; Coe, J. V.; Tuttle, T. R. The Proton's Absolute Aqueous Enthalpy and Gibbs Free Energy of Solvation from Cluster-Ion Solvation Data. *J. Phys. Chem. A* **1998**, *102*, 7787−7794.

(128) Camaioni, D. M.; Schwerdtfeger, C. A. Comment on "Accurate Experimental Values for the Free Energies of Hydration of H$^+$, OH$^-$, and H$_3$O$^+$". *J. Phys. Chem. A* **2005**, *109*, 10795−10797.